Membrane Composition and Raf[CRD]-Membrane Attachment Are Driving Forces for K-Ras4B Dimer Stability

Ioannis Andreadelis[1], Sofia Kiriakidi,[1] Christos Lamprakis[1], Anastasia Theodoropoulou[1], Stefan Doerr[1], Alexios Chatzigoulas[1], John Manchester[2], Camilo Velez-Vega[2], José S. Duca[2,*], Zoe Cournia[1,*]

[1]Biomedical Research Foundation, Academy of Athens, 4 Soranou Ephessiou, 11527 Athens, Greece

[2]Computer-Aided Drug Discovery, Global Discovery Chemistry, Novartis Institutes for BioMedical Research, 100 Technology Square, Cambridge, Massachusetts 02139, United States

E-mail: jose.duca@novartis.com, zcournia@bioacademy.gr

Phone: +30 210 6597 195

Abstract

RAS proteins are membrane-anchored GTPases that regulate key cellular signaling networks. It has been recently shown that different anionic lipid types can affect the properties of RAS in terms of dimerization/clustering on the cell membrane. To understand the effects of anionic lipids on key spatiotemporal properties of dimeric K-Ras4B, we perform all-atom molecular dynamics simulations of the dimer K-Ras4B in the presence and absence of Raf[CRD/RBD] effectors on two model anionic lipid membranes: one containing 78% mol. DOPC, 20% mol. DOPS, 2% mol. PIP2 and another one with enhanced concentration of anionic lipids containing 50% mol. DOPC, 40% mol. DOPS, 10% mol. PIP2. Analysis of our results unveils the orientational space of dimeric K-Ras4B, and shows that the stability of the dimer is enhanced on the membrane containing a high concentration of anionic lipids in the absence of Raf effectors. This enhanced stability is also observed in the presence of Raf[CRD/RBD] effectors although it is not influenced by the concentration of anionic lipids in the membrane, but rather on the ability of Raf[CRD] to anchor to the membrane. We generate dominant K-Ras4B conformations by Markov State Modeling and yield the population of states according to the K-Ras4B orientation on the membrane. For the membrane containing anionic lipids, we observe correlations between the diffusion of K-Ras4B and PIP2 and anchoring of anionic lipids to the Raf[CRD] domain. We conclude that the presence of effectors with the CRD domain anchoring on the membrane as well as the membrane composition both influence the conformational stability of the K-Ras4B dimer enabling the preservation of crucial interface interactions.

1. Introduction

Ras proteins are plasma membrane associated GTPases that act as signal transducers switching between the active (GTP bound) and inactive (GDP bound) states; in their active state, GTPases interact with effector proteins facilitating different downstream signaling pathways necessary for cell proliferation/growth[1]. The upstream regulatory guanine nucleotide exchange factor (GEF) proteins activate GTPases by enabling the release of GDP to allow binding of GTP, while GTPase deactivation is mediated by the GTPase activating proteins (GAPs), which include GTP hydrolysis[2]. Single point mutations on Ras proteins at the positions of association with these regulatory proteins (primarily at codons 12, 13, and 61) result in permanent GTPase activity on the plasma membrane, which is associated to nearly 30% of human tumors.[2,3] Consequently, over the last decade direct drug targeting of Ras signaling has been a popular albeit challenging strategy for developing cancer therapeutics[4]. Ras proteins share a conserved G-domain[5] and a cationic hypervariable region (HVR), which enables association with the membrane through its C-terminal post translational modification.[6,7]

K-Ras4B is one of three Ras isoforms, which stimulates the extracellular signal-regulated kinases (ERK)/mitogen-activated protein kinase (MAPK) pathway by recruiting rapidly accelerated-fibrosarcoma (Raf) kinases to membranes.[8,9] Cytosolic Raf exists in an inactive, auto-inhibited conformational state, which is activated upon binding to K-Ras4B[10]. Raf kinases consist of the kinase domain connected by a long linker to the Ras Binding Domain (RBD), which directly binds to the effector binding domain of K-Ras4B,[11] as well as the Cysteine Rich Domain (CRD), a membrane binding domain.[12] Upon binding to the K-Ras4B dimer, the kinase domains of Raf interact through a dimer interface, mediated by K-Ras4B on the cell membrane (Figure S1), and their association leads to the phosphorylation and activation of MAPK, transmitting the signal down to ERK.[13] Thus, the activity of the resulting K-Ras4B-Raf[RBD/CRD] membrane anchored protein complex is regulated by the dimerization of the K-Ras4B G-domain.[14,15] The existence of K-Ras dimers has been confirmed by a number of studies[14-16,17] as well as a study observing a trimer conformation[18]. Apparently, dimerization is critical for the activity of wild-type (WT) K-Ras and its oncogenic variant G12D K-Ras as shown by the fact that the K-Ras D154Q mutant does not have the ability to dimerize[16], being unable to activate downstream signaling and cell growth *in vitro* and *in vivo* both in the WT and mutant forms.

Different dimer interfaces have been proposed for membrane-bound RAS dimers such as the region between the α4-α5 helices and the loop between β2-β3 sheets for NRAS,[19] the α4-β6-α5 helical interface for HRAS,[20] the α4-α5 interface,[16,17,21] the β2 strands or the α3-α4 helical interface for KRAS.[15,22] Moreover, Ras dimers have been pursued in experimental studies and are resolved by X-ray crystallography though in the absence of the cell membrane[23,24] as well as by NMR-inspired structures in nanodiscs.[17] The α4-α5 interface has been identified as highly likely for K-Ras4B dimers, as demonstrated in a study showing that

disrupting the α4-α5 interface by introducing the D154Q mutant abolished both WT and mutant KRAS homodimerization[16] but did not influence K-Ras4B intrinsic GTPase activity, GEF or GAP sensitivity, and C-Raf binding. Specifically, the α4-α5 dimer interface present in the asymmetric unit of the PDB crystal structure 5VQ2,[23] residues D154 and R161 of the two different K-Ras4B monomers form two intermolecular salt bridges; abolishing this interaction by introducing the D154Q mutation interrupts K-Ras4B dimerization.[16] Moreover, a second study demonstrated that a designed monobody interacts with the catalytic domain of both GTP- and GDP-bound KRAS and disrupts KRAS dimerization through the α4-α5 interface.[20] Another recent study on nanodiscs via paramagnetic relaxation enhancement (PRE) NMR also reported the α4-α5 region as the likely dimerization interface, but proposed a different orientation of K-Ras4B membrane-associated homodimers bound to GTP and GDP.[17] A combination of size exclusion chromatography and small angle X-ray scattering (SAXS) experiments showed that the presence of Raf[RBD] is sufficient to promote Ras G-domain dimerization in solution and that the molecular envelopes generated from the SAXS data unequivocally support a dimeric Ras/Raf[RBD] structure which fits to the α4-α5 interface.[25] These observations suggest that the α4-α5 interface may be the most viable for K-Ras dimerization; however, a conclusive biologically-relevant K-Ras4B dimer structure has not been yet established.

Prior to Raf binding, the K-Ras4B G-domain adopts distinct orientational conformations relative to the anionic membrane.[26] In some of these configurations the membrane occludes binding of the Raf effector as well as influences the dynamics of dimerization.[27,28] An interplay between the presence of specific anionic lipid species in the local environment of K-Ras4B, the conformations of the HVR,[29] and its influence on the dynamics of the G-domain control the reorientation and diffusion of K-Ras4B on the cell membrane, affecting both the assembly of the complex as well as its dimerization.[30] The phosphatidylserine (PS) and phosphatidylinositol 4,5-bisphosphate (PIP2) are the signature anionic lipid species that play a critical role in affecting Ras conformations on the plasma membrane. Even though the total concentration of PIP2 in the plasma membrane is below 1%, this average does not give a clear picture of the local PIP2 concentration in the cellular membrane because PIP2 and other phosphoinositide lipids are in fact distributed non-uniformly in the plasma membrane. Studies on the protein MARCKS show that in its vicinity, the local PIP2 concentration can indeed be elevated by a factor of 400, using a cluster of basic residues that creates a significantly positive electrostatic potential, which enhances the local concentration of PIP2 by creating a basin of attraction for anionic lipids.[31] As already suggested in the literature, similar to the MARCKS protein, the basic cluster of K-Ras could laterally sequester and concentrate PIP2 molecules.[32] The influence of PIP2 and PS lipids in the interaction of the HVR and the G-domain with the plasma membrane has been studied both computationally and experimentally,[29 33 34 35 36] revealing their impact in the K-Ras4B localization on the plasma membrane. In a recent review, where the diverse PIP2 functions at the plasma membrane are explored,[37] studies using super-resolution stimulated-emission depletion (STED)

microscopy are reported, which indicate that PIP2 forms clusters on the cellular membrane that reach 65-73 nm in size.[38 39] Following these indications for local PIP2 aggregation, recent studies on K-Ras have been conducted, where increased PIP2 concentration is used in order to model this raft formation in the vicinity of the receptor. Particularly, a multi-microsecond MD study exploring the K-RAS isoform 4A orientation with respect to the membrane composition has used a PIP2 concentration of 5.3% mol for one of the studied model membranes.[40] In this study, a clustering of PIP2 molecules in contact or nearby the K-Ras4A-membrane contact region has been observed throughout the simulation time, where several PIP2 molecules were found to interact with positively charged residues of K-Ras4A. Because the inositol phosphate group has several substituents, a PIP2 molecule is able to interact with different K-Ras4A residues simultaneously, thus engaging in very stable interactions. A comprehensive list of residues interacting with PIP2 can be found in ref.[40] .Moreover, the POPC/PIP2 membrane employed in this study has a broader charge distribution than the POPC or POPC/POPS membrane systems due to the additional charged phosphate groups carried by the PIP2 inositol headgroup. This broader charge distribution leads to diverse K-Ras4A orientations towards the membrane as these orientations are mostly dictated by the electrostatic attraction between charged residues and the lipids. Moreover, a recent 1ms MD study that addresses how the spatiotemporal properties of K-Ras4B are affected by anionic lipids has employed model membranes that reach an 8% mol. PIP2 concentration,[30] suggests that the sequestration dynamics of PIP2 can strongly affect the dynamics of K-Ras4B by interacting with the HVR region, which has 11 lysine and only two acidic residues. Indeed, the lateral diffusion of PIP2 appears to have a stronger correlation with the diffusion of K-Ras4B than the lateral diffusion of POPS and K-Ras4B diffuses slower in membranes containing PIP2. Another MD study performed on nanodiscs, investigated several membrane compositions including one with a PIP2 concentration of up to 10% mol. This study showed that K-Ras4B/membrane dissociation constant in membranes with 10% mol. PIP2 concentration is decreased nearly 10-fold relative to membranes that contained only 3% mol. PIP2.[35] Additionally, in a recent study combining NMR spectroscopy with MD simulations complemented by biophysical- and cell-biology assays, membranes containing 5% mol. PIP2 in DOPC nanodiscs were employed and the β2-β3 strands and helices α4 and α5 of the K-Ras4B G-domain were found to bind to PIP2.[34] All studies showed that K-Ras orientation on model membranes is highly affected by the overall negative charge of the membrane and also by the type of lipid interacting with K-Ras, pinpointing that a putative high PIP2 concentration in the vicinity of K-Ras should be thoroughly examined for its effects on the structure and dynamics of the protein. For these reasons, in this study we have chosen to study K-Ras4B in the presence of both a low (2% mol.) and a high (10% mol.) PIP2 concentration model membrane.

Recent NMR studies of the K-Ras4B dimer without effectors[17] and of the K-Ras4B-Raf[RBD/CRD] monomer[41] on the plasma membrane report distinct possible orientations for the G-domain on the membrane. At the same time, the membrane composition as well as the competition for protein-membrane contacts between

the CRD domain of Raf and K-Ras4B are key factors affecting the K-Ras4B configurational ensemble on the membrane and could enhance dimer stability.[42] Integrating structural and computational studies could exploit the relationship between the disruption of K-Ras4B signaling, the occlusion of the effector binding domain, and specific lipid species for drug design.[43] In this study, the K-Ras4B-Raf[RBD/CRD] dimer is modeled in a conformation in accordance to the α4-α5 interface anchored on two model plasma membranes with compositions of 78:20:2 %mol. and 50:40:10 %mol. DOPC:DOPS:PIP2 in order to examine the influence of anionic lipid concentration on the stability of the K-Ras4B dimer in the presence and absence of Raf[RBD/CRD] effectors. The distribution of lipid species as well as their interactions with the different domains of the protein complex is studied with respect to the varying PIP2 concentration. We find that the stability of K-Ras4B on the model membrane in the absence of effectors is influenced by the anionic lipid concentration. In the presence of effectors, the system shows enhanced stability compared to the no effector system, and this stability is not further enhanced with the increase of anionic lipids. Furthermore, we examine the diffusion of K-Ras4B and the different lipids. We calculate the relevant K-Ras4B dimer macrostates for each system and present the population of states according to the K-Ras4B orientation on the membrane. Through these results, we establish key components that may facilitate K-Ras4B dimer stability.

2. Methods

2.1 Building the K-Ras4B Dimer Structure with and without Effectors on Model Membranes

Biochemical data point to the α4-α5 interface being the most viable for K-Ras4B dimerization, based on experimental evidence showing that the D154Q mutation abolishes both the WT and mutant K-Ras dimerization without influencing its intrinsic GTPase activity, GEF or GAP sensitivity and C-Raf binding,[16] and also based on the recently published molecular model of K-Ras4B. The same interface is also present in a K-Ras4B dimer model built using the PDB ID: 4DSO structure[44] using paramagnetic relaxation enhancement (PRE) NMR-derived distances and a multibody docking protocol via HADDOCK 2.2.[17] In the crystal structure of Ref.[23] (PDB ID: 5VQ2) α5 is rotated 90^{o} with respect to α4 and α5 helix of the opposite monomer, forming an α4-α5 interface, which includes α5-α5 and α4-α4 interfaces with the two intermolecular salt bridges forming between R161 and D154 (Figure S2).

The asymmetric unit in Ref.[23] is the only crystal structure of a K-Ras4B dimer conformation that exists to date in complex with GTP. This conformation is also consistent with the α4-α5 interface hypothesized to be the main dimer interface contact in Ref.[16] In order to assess the stability of this interface, we first performed short dimer binding simulations with varying orientations starting from two K-Ras4B monomers, bound to a model membrane at a distance of at least 10 Å (see the Supporting Information for more information). The initial orientations for these simulations were modeled after crystal structures (e.g., PDB

ID 5VQ2[23]), previously proposed interfaces from the literature,[15] or potential dimer configurations that we identified by means of solvent simulations of two unbound K-Ras monomers (see Supporting Information). The only orientation that displayed stable interactions was the one corresponding to the 5VQ2 crystal structure, as also proposed in Ref.[16] , and hence it was chosen as the best candidate for the K-Ras4B dimer interface. The full structure of the K-Ras4B monomer was generated using 5VQ2[23] as the core and 4G0N[24] and 2MSC[28] to build the missing regions of K-Ras4B. To build the Raf RBD and CRD effector models we used structures with PDB IDs 4G0N and 1FAQ[45] and subsequently coupled them to K-Ras4B to generate the final GTP-bound complex (see Figure S3 the Supporting Information for a schematic description of model building). The modelled Raf/Ras complex presented herein is in excellent agreement with the recent crystal structures of WT and oncogenic mutants of KRas-4B complexed with the RBD and membrane-interacting CRD domains published by Tran et al.[46] A superposition of our modelled structure with the structure published by Tran for the KRas-4B G12V mutant (PDB ID: 6XHA) yields an RMSD of only 1.87 Å if the Raf[CRD] region is omitted, as this domain is positioned in the crystal structure in a non-compatible conformation with the membrane location, which could be an artifact arising from crystal packing. We also compared the structure published by Tran et al.[46] with the structure recently published by Cookis and Mattos (PDB ID: 7JHP)[21] or the WT H-RAS; superposition of the two structures shows an RMSD of only 0.75 Å as they both have a CRD domain pointing away from the membrane. A detailed comparison of our model K-Ras4B structure with the crystal structures mentioned above is illustrated in Figure S4.

Model membranes were created for the simulations of the K-Ras4B dimer. The first membrane was constructed with a lipid composition of 78% mol. DOPC, 20% mol. DOPS, 2% mol. PIP2 (henceforth called 78:20:2 membrane) and the second one with a higher concentration of the negatively charged DOPS and PIP2 lipids, namely 50% mol. DOPC, 40% mol. DOPS and 10% mol. PIP2 (henceforth called 50:40:10 membrane). The K-Ras4B-Raf[RBD/CRD] dimer model was then placed on the membrane, and the farnesyl groups were inserted into the membrane and oriented vertically to the membrane plane adopting six different orientations (see Methods and Supporting Information for more information) for the 5VQ2-based model. We then run four replica simulations of the dimer K-Ras4B bound to the membrane without Raf effectors in the 78:20:2 as well in the 50:40:10 membrane, six replica simulations of the dimer K-Ras4B bound to the membrane with Raf[RBD/CRD] effectors on the 78:20:2 membrane and two replica simulations of the dimer K-Ras4B bound to the membrane with Raf[RBD/CRD] effectors on the 50:40:10 membrane. Simulations were carried out with the ACEMD3 software[47] and the CHARMM36m force field.[48] For more details on the simulation protocol please refer to the Supporting Information. All replica simulations mentioned in this manuscript are simulations of the exact same system starting with different initial velocities for each independent run and are listed in Table S1.

2.2 Markov State Models of the K-Ras4B and K-Ras4B/Raf Conformational Space

Markov State Models (MSMs) were constructed in order to explore the K-Ras4B and K-Ras4B/Raf[RBD/CRD] conformational space with respect to the membrane for both membrane models. The trajectories were projected to the metric space defined by the distance of the Cα atoms of both K-Ras4B monomers and the P atoms of the PIP2 molecules (P as defined by CHARMM36m) for the membrane containing 10% mol. PIP2 and the P atoms of both PIP2 and DOPC molecules (P as defined by CHARMM36m) for the membrane containing 2% mol. PIP2, in order to explore the conformational space of the dimer with respect to the model membranes. Time Dependent Component Analysis (TICA) was performed on the projected trajectories on 100 dimensions with a lag time of 0.1 ns for all systems. Clustering with the k-means algorithm followed to discretize the TICA space using 30 cluster centers for all systems. The MSMs were constructed using the PyEMMA algorithm[49] with a lag time of 3 ns for the 78:20:2 membrane and K-Ras4B/Raf[RBD/CRD] system, 5 ns for the 78:20:2 membrane and K-Ras4B system, 4 ns for the 50:40:10 membrane and K-Ras4B/Raf[RBD/CRD] system and 1 ns for the 50:40:10 membrane and K-Ras4B system without effectors. A Perron-Cluster Cluster Analysis was then performed using the PCCA+ algorithm[50] to assign the aforementioned clusters in 4 macrostates for the 78:20:2 membrane and K-Ras4B/Raf[RBD/CRD] system and 3 macrostates for the rest of the systems. A detailed description of the MSM construction is provided in the Methods section of the Supporting Information; the relevant Chapman-Kolmogorov tests, implied timescales, energy surfaces and kinetic models[51] are presented in Supporting Information Figures S5 and S6. The MSM macrostates are provided as pdb structures in the Supporting Information data.

2.3 Analyses

The diffusion of K-Ras4B, DOPC, DOPS, and PIP2 molecules was calculated by means of Mean Square Displacement (MSD) using GROMACS module gmx_msd.[52] The diffusion coefficients were calculated using the Einstein relation and fitting was performed in the linear regime of the log-log MSD(t) plot as described in Ref.[53]. Errors represent standard deviations calculated by block averaging with the gmx_analyze module. Radial pair distribution functions (RDFs) were calculated using the VMD gofr plugin[54] for the a) Cα atom of residue T183 of HVR and b) the NZ atom of K148 with respect to the P atoms of DOPC, DOPS and PIP2 (atom names as defined in CHARMM36m). Integration of the RDFs was performed in order to calculate the number of lipids that are present up to 10 Å using the number integral over g(r) as implemented in the gofr plugin. Error bars are included based on the standard deviation between each replica. The percentage of K-Ras4B G-domain membrane contacts was computed with the contact Freq.tcl script of VMD. Hydrogen atoms were omitted in this calculation and a contact was counted when two examined atoms were distanced below 5 Å. The secondary structure analyses of the proteins were performed with the timeline plugin of VMD that uses the algorithm STRIDE or protein secondary structure assignment from atomic coordinates based on the combined use of hydrogen bond energy and statistically derived backbone torsional angle information.[55] Trajectories were clustered using the gmx_cluster module and the linkage method, where a structure is added to a cluster when its distance to any element of the cluster is less than

a cutoff distance set to 0.1 nm. The relative orientation of CRD with resect to K-Ras4B was computed using the GROMACS gmx gangle module with vectors defined as described in Figure S7. Contour plots showing the probability of K-Ras4B states with respect to their membrane orientation were constructed by plotting the angle between the K-Ras4B α5 helix and the membrane plane along with the distances of the geometric center of each K-Ras4B monomer to the geometric center of the membrane. The populations are calculated by dividing the number of each state by the total number of sampling frames and then normalize the resulting histograms.

3. Results and Discussion

3.1 Membrane-Bound K-Ras4B Dimer in the absence of Effectors Shows Enhanced Flexibility in the 78:20:2 Membrane Compared to the 50:40:10 Membrane

The initial dimer configuration was selected after performing short K-Ras4B dimer binding simulations with varying orientations starting from two K-Ras4B monomers without Raf effectors. This procedure identified the PDB ID 5VQ2 structure as the most stable structure (see Methods section and Supporting Information). We then performed all-atom MD simulations of the membrane-bound K-Ras4B dimer using 78:20:2 %mol. and 50:40:10 %mol. DOPC:DOPS:PIP2 membranes (Table S1). The K-Ras4B dimer interface based on the 5VQ2 structure is stabilized by two intermolecular salt bridges between residues R161 and D154 belonging to two different monomers (see Figure S2 for a schematic of the salt bridges). We thus investigated the conformational flexibility of the dimer as well as the stability of the two intermolecular salt bridges formed on the dimer α4-α5 interface between residues D154 and R161. The RMSD time series of these dimers relative to their respective initial conformations is stabilized after ~400 ns (Figure S8) throughout the simulations. Moreover, visualization of the system showed that in all cases K-Ras4B without effectors tilts relative to the membrane normal and lies towards the membrane plane (Figure 1, upper panel). This dimer tilting is dynamic, leading to both K-Ras4B monomers contacting the membrane through α2, α3 and α4 helices or loop 7 (Figure 1 and FigureS9).

Next, we investigated the stability of the K-Ras4B dimer in the absence of the Raf effector on the 50:40:10 membrane, in order to assess whether it led to results analogous to those observed for the 78:20:2 membrane. We found that the RMSD values are overall more stable in the 50:40:10 membrane (average RMSD = 1.9 ± 0.5 Å, Figure S8, right) compared to the 78:20:2 membrane (average RMSD = 2.8 ± 0.8 Å, Figure S8, left). Moreover, the salt bridges between D154 and R161 at the dimer interface is stable throughout the simulations for the 50:40:10 membrane, while it significantly fluctuates for the 78:20:2 membrane (Figure 2). The stability of the salt bridges for the K-Ras4B dimer in the case of the 50:40:10 membrane can be attributed to the enhanced K-Ras4B-membrane contacts as shown in Figure 1. Figure 1 shows that when the membrane contains 50% mol. anionic lipids (40% mol. DOPS and 10% mol. PIP2), the α2 and α3 helices contact the cell membrane at a higher percentage compared to when the membrane

contains only 22% mol. anionic lipids (20% mol. DOPS and 2% mol. PIP2). Loop 7 of K-Ras4B (residues 105 to 109) contributes to G domain-membrane interactions in both membrane systems. This result is consistent to Ref.[26], where loop 7 is considered as a toehold that aids the catalytic domain of K-Ras rock between the surfaces located at helices α3/4 and βstrands 1–3/helix α2. Conversely, with a 2% mol. PIP2 concentration, contact between the membrane and α2 is minimal. In the case of the 50:40:10 membrane, K-Ras4B remains stable and does not show a tendency to tilt toward the membrane, unlike in the 78:20:2 membrane. A comparison of the frequency of contacts between K-Ras4B-membrane for both K-Ras4B monomers with the two model membranes can also be seen in Figures S9 and S10. However, there was no significant difference in the RMSF plots of K-Ras4B for the two different membrane systems, except the switch II region (amino acids 60-70), where K-Ras4B mutations are located (as well as in the P-loop); switch II is more flexible in the K-Ras4B residing on the 50:40:10 membrane (Figure S11).

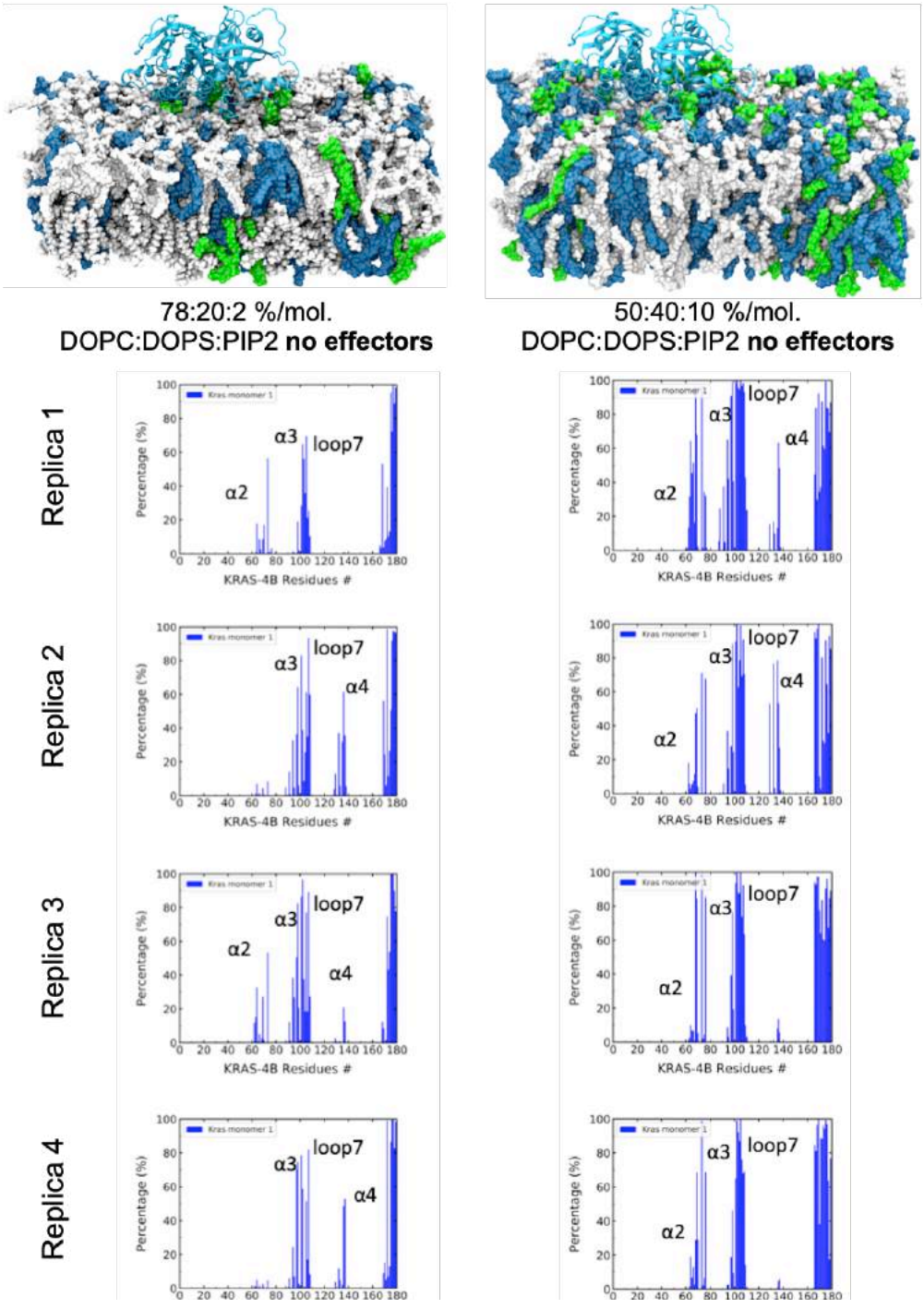

Figure 1. Snapshots of orientations of K-Ras4B dimer on the membrane without effectors (upper panel). Percentage of K-Ras4B-membrane interactions of the K-Ras4B dimer based on the 5VQ2 structure with no effectors in the 78:20:2 and 50:40:10 membrane for the first K-Ras4B monomer (monomer 1, KR1). The other K-Ras4B monomer (monomer 0, KR0) results are shown in Figures S9 and S10. Figure S12 shows snapshots of representative orientations of K-Ras4B in contact with the two membrane models.

The conformational flexibility of K-Ras4B monomers in the absence of Raf effectors triggers an overall instability of the interactions along the dimer interface, including loss of the salt bridges between D154 and R161 at the dimer interface (Figure 2) in three out of the four replica simulations in the 78:20:2 membrane. This disruption of the α4-α5 dimer interface is observed after 0.3 μs (replica 1), throughout the whole 1 μs trajectory (replica 2) or in one of the salt bridges in replica 4 in the dimer K-Ras4B systems without Raf effectors bound to a 78:20:2 membrane. These observations are in close agreement with reported studies suggesting that K-Ras4B gains dimerization capability only in the presence of additional factors, i.e. downstream effectors such as Raf.[56] On the contrary, these salt bridges are stable throughout 1μs for all replica simulations in the 50:40:10 membrane even in the absence of Raf effectors, indicating that the added negatively charged lipids confer additional stability to the α4-α5 K-Ras4B interface.

In order to further investigate the K-Ras4B conformational changes that take place throughout the trajectories, we constructed MSMs combining the trajectories of all replica simulations (a total of 4 μs for each membrane model). The feature used in order to project the trajectories was the distance between the α5 helices of each K-Ras4B monomer and the P atoms of PIP2 (for the 50:40:10 membrane) or the PIP2 and DOPS lipid molecules (for the 78:20:2 membrane, atom names as defined in CHARMM36m). More details regarding the construction of MSMs are provided in the Methods section and Supporting Information Section 1.4.

The MSMs constructed for the 78:20:2 membrane-K-Ras4B in the absence of Raf effectors yielded three similar macrostates (RMSD = 4.1 ± 0.8 Å) indicating that the cumulative 4 μs trajectories used to construct the models explored a very stable area of the phase space (Figure 3). These structures are tilted towards the membrane plane and the salt bridges that were present in the initial K-Ras4B (based on the PDB ID 5VQ2 structure) are not retained. The MSM macrostates reflect the D154-R161 salt bridge breaking discussed above for this system. With respect to the 50:40:10 membrane-K-Ras4B in the absence of Raf effectors, the MSMs yielded again three similar macrostates (RMSD = 6.2 ± 0.2 Å) although in this case all states retain the salt bridges at the α4-α5 interface, with an average salt bridge distance of 4.1 ± 0.4 Å indicating a more stable system compared to the 78:20:2 membrane system.

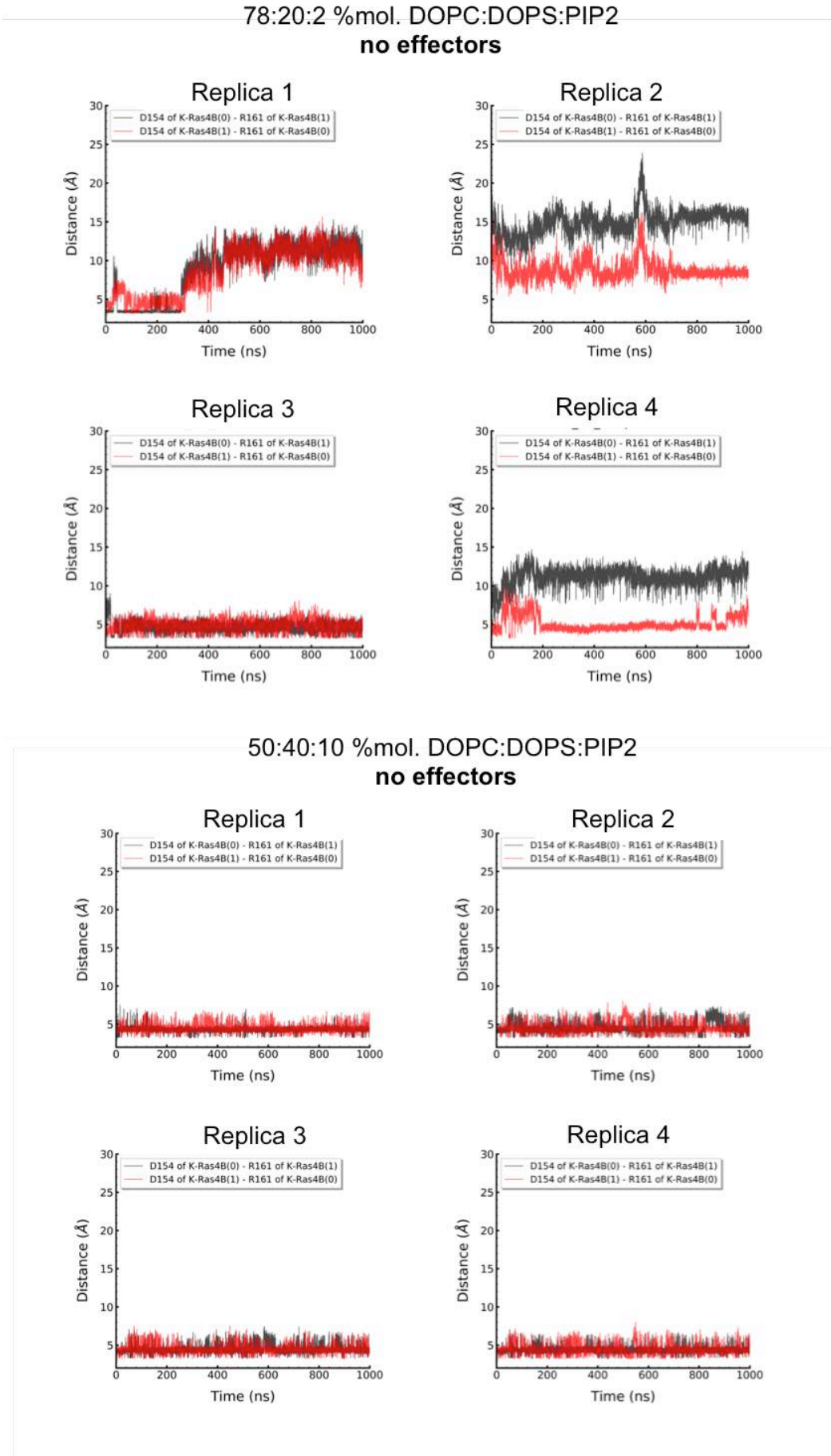

Figure 2. Distance of salt bridges between D154 and R161 for the K-Ras4B dimer without effectors on a 78:20:2 or a 50:40:10 membrane for all independent runs.

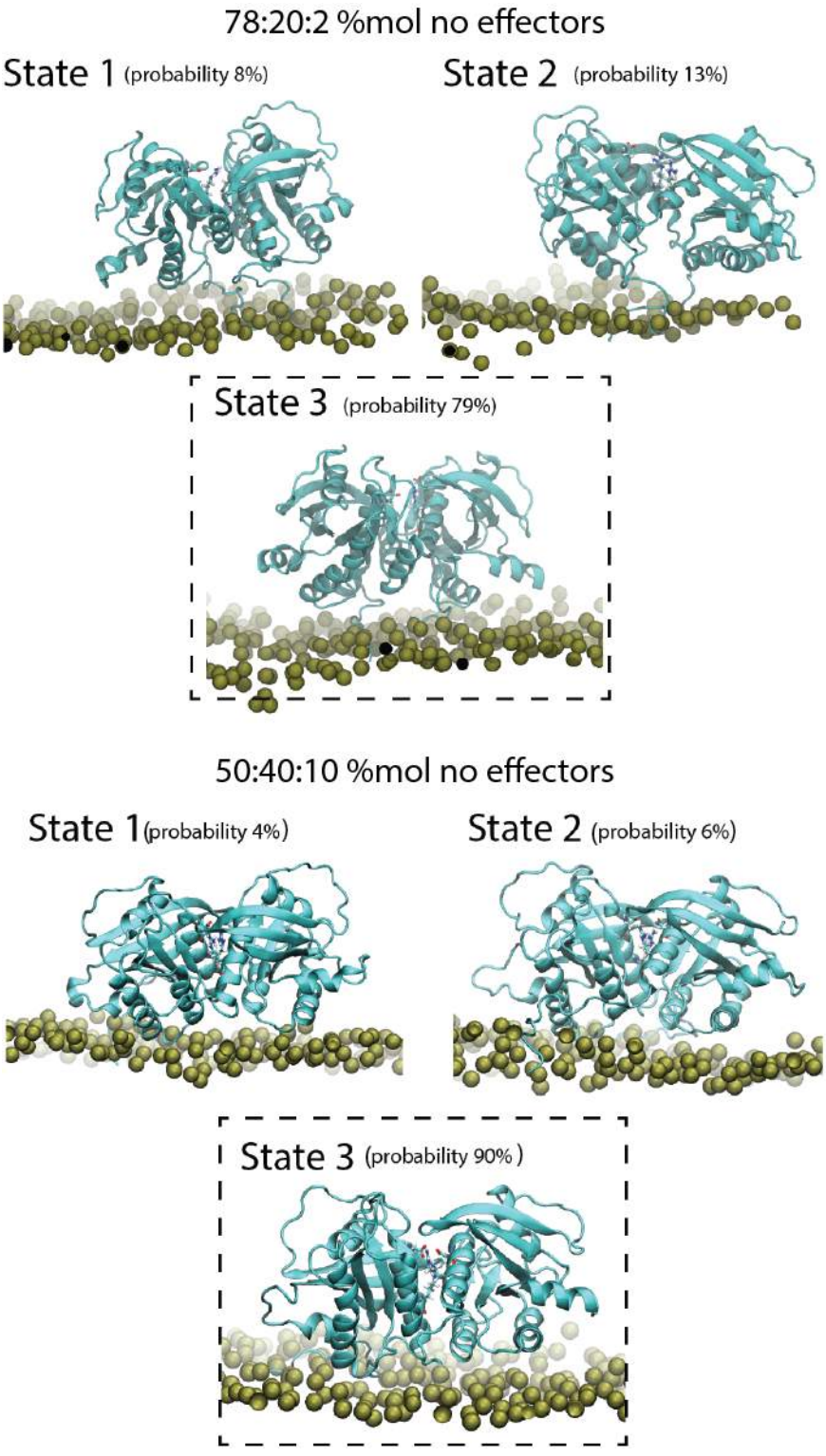

Figure 3. K-Ras4B macrostates calculated with MSMs. For the 78:20:2 membrane with K-Ras4B in the absence of Raf effectors, the most probable conformation is State 3 (79%), where one K-Ras monomer is tilted towards the membrane and the salt bridges between D154 and R161 are broken. For the 50:40:10 membrane with K-Ras4B in the absence of Raf effectors, the most probable conformation is State 3 (90%) with stable salt bridges at the dimer interface.

A cross-validation of the most characteristic K-Ras4B conformation was performed by constructing contour plots, showing the population of states according to the K-Ras4B orientation with respect to the membrane. The results are in very good agreement with the most probable K-Ras4B conformation resulting from the MSM analysis, both for the 78:20:2 and the 50:40:10 membrane K-Ras4B systems without effectors, as illustrated in Figure 4. The white rectangles represent the relevant K-Ras4B/membrane distance and K-Ras4B α5 helix/membrane plane angle for macrostate 3, and are located at the highest probability areas of the contour plot.

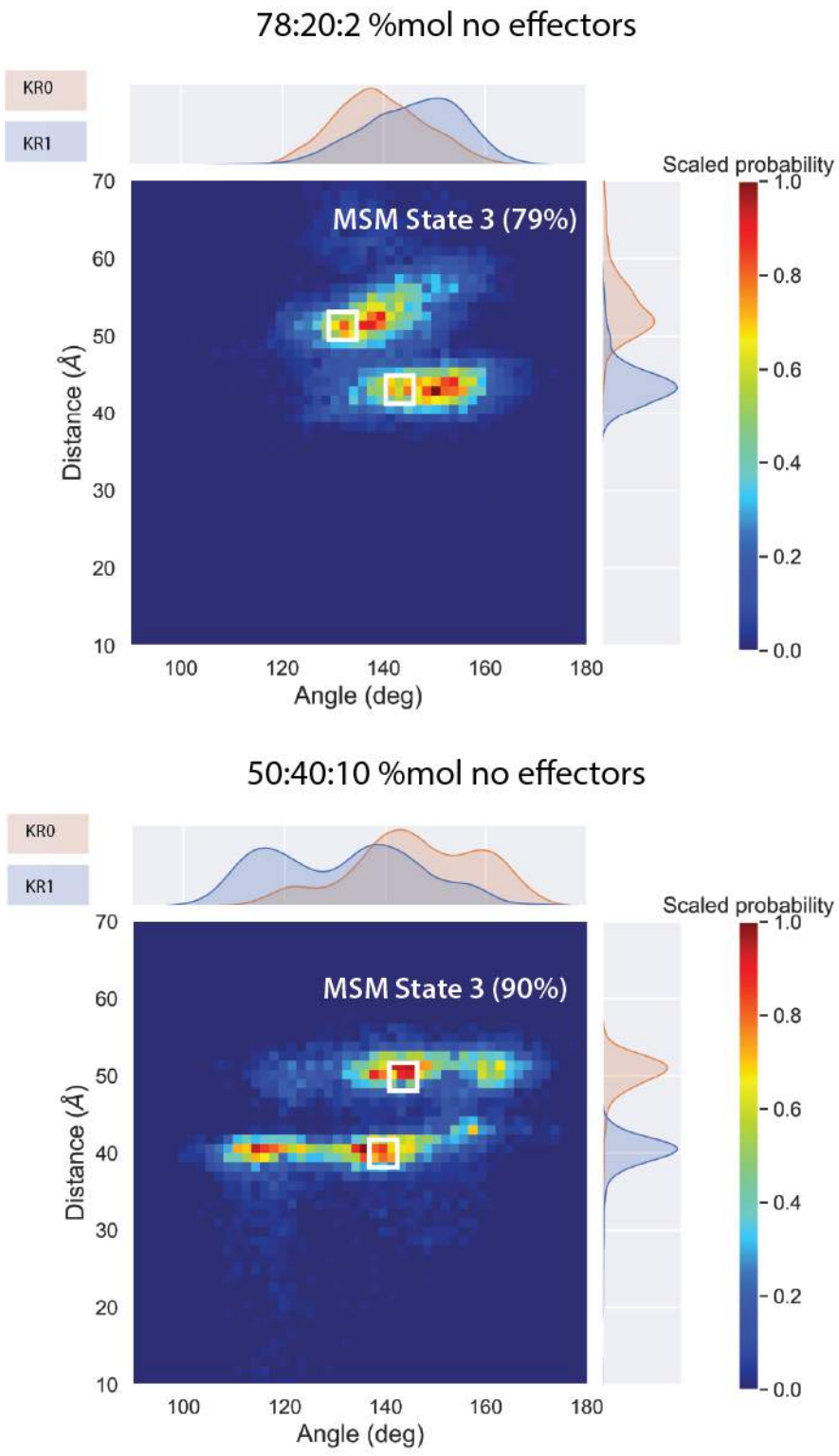

Figure 4. Contour plots showing the population of K-Ras4B states with respect to their membrane orientation for 78:20:2 (top) and 50:40:10 (bottom) membranes without Raf effectors. The computed distance corresponds to the distance between the geometric center of each K-Ras4B monomer and the bilayer geometric center, whereas the computed angle corresponds to the angle of each K-Ras4B α5 helix with respect to the membrane plane. The white rectangles correspond to the relevant distances and angles of the most probable metastable states calculated from MSMs (see the Supporting Information). Distance and angle histograms of the two K-Ras4B monomers are illustrated in pink (KR0) and light blue (KR1).

In addition, cluster analysis of each model system was performed for all trajectories and representative structures are presented in Figure S13. In the 78:20:2 membrane, residues 166-172 of the α5 helix of one of the monomers is folded, whereas in the 50:40:10 membrane, these residues are unfolded in both monomers are leaning towards the membrane.

3.2 Membrane-Bound K-Ras4B Dimer in the Presence of Raf Effectors Shows Stability Irrespective of the Model Membrane Anionic Lipid Concentration

Next, we sought to study the conformational stability of K-Ras4B dimers in the presence of the Raf effector domains that contact K-Ras4B, i.e. the RBD and the CRD domains of Raf. Initially, we performed six independent MD simulations of K-Ras4B dimer bound to Raf on a 78:20:2 membrane, each with a different HVR configuration, in order to investigate if any of these arrangements contributes to stable CRD-membrane interactions. These simulations are labelled as "Simulation 0-5" (see Table S1 for a list of simulations performed). Overall, K-Ras4B dimers bound to Raf[RBD/CRD] demonstrate more conformational stability (RMSD = 2.2 ± 0.7 Å, Figure S14) in the 78:20:2 membrane compared to the K-Ras4B dimer in the absence of the Raf effector, excluding simulations 2 and 5, where the CRD of Raf detaches from the membrane. The CRDs remain anchored to the membrane in the rest of the simulations. This CRD detachment influences the stability of K-Ras4B dimer on the membrane, with simulation #5 presenting the largest instability (RMSD of K-Ras4B$^{1\text{-}165}$ Cα atoms ≈ 5 Å). The RMSD of K-Ras4B dimers in the 50:40:10 membrane is similar (RMSD = 2.4 ± 0.9 Å, Figure S15), therefore, in this case, the added negatively charged lipids do not confer any additional stability to the K-Ras4B dimer. The RMSF plots of K-Ras4B in both membrane types (Figures S16-S17) show that the switch II region is again the most flexible with a more pronounced effect in the 78:20:2 membrane.

Moreover, as expected, the K-Ras4B stability is also reflected on the dimer interface interactions and particularly on the salt bridges formed between D154 and R161 of the two K-Ras4B monomers (Figure 5). In simulations 2 and 5, the CRD is detaching from the membrane, leading to a complete disruption of the interface between the two monomers through interactions between the α5 helices of the two monomers (Figure S2). In simulations 0, 1, 3, 4, where the CRD remains anchored on the membrane, the salt bridges retain their stability. Hence, the decisive factor for maintaining K-Ras4B dimer stability in the presence of effectors is the ability of the CRD to remain anchored on the membrane. Therefore, the conformational stability of K-Ras4B suggests that the presence of the effector provides conformational restriction to K-Ras4B and alleviates K-Ras4B-membrane interactions by limiting the accessible K-Ras4B areas that may contact the cell membrane by steric hindrance.

Next, we sought to investigate whether the increase in the concentration of negatively charged lipids in a 50:40:10 membrane will influence the stability of the K-Ras4B dimer in the presence of Raf[RBD/CRD] effectors. Again, the decisive factor for interface stability of the K-Ras4B dimer is the stability of the Raf[CRD] domain. As can be seen in Figure 5, in replica 1 of the K-Ras4B dimer in the 50:40:10 membrane, where the CRDs detach from the membrane, the stabilizing salt bridges at the dimer interface are lost, while in replica 2, where the CRD is anchored on the membrane, the salt bridges are retained. The increase in the negatively charged phospholipid concentration (50% mol. vs. 22% mol. between the two membrane systems studied herein) does not confer additional anchoring to the CRD, however, Figure 6 shows that the percentage of K-Ras4B-membrane interactions of the K-Ras4B dimer with Raf[RBD/CRD] effectors on the 78:20:2 and 50:40:10 membranes differs significantly. The K-Ras4B dimer with Raf[RBD/CRD] effectors on the 50:40:10 membrane contacts the membrane with its α2 and α3 helices and loop 7. To investigate this further, we calculated the radial distribution functions of T183 of the HVR (Cα atom) with respect to the phospholipids (P atom) as well as of K148 of the CRD domain (NZ atom), which is known to anchor to the membrane with respect to the phospholipids (P atom). Our results show that when the number of anionic lipids are increased (from 22% in the 78:20:2 to membrane to 50% in the 50:40:10 membrane) both anionic species gather around the positively charged nitrogen atom of K148 of CRD (Table 1). For T183 of the HVR, the DOPC lipids in its vicinity are replaced by DOPS and the number of PIP2 remains unchanged (Table 2).

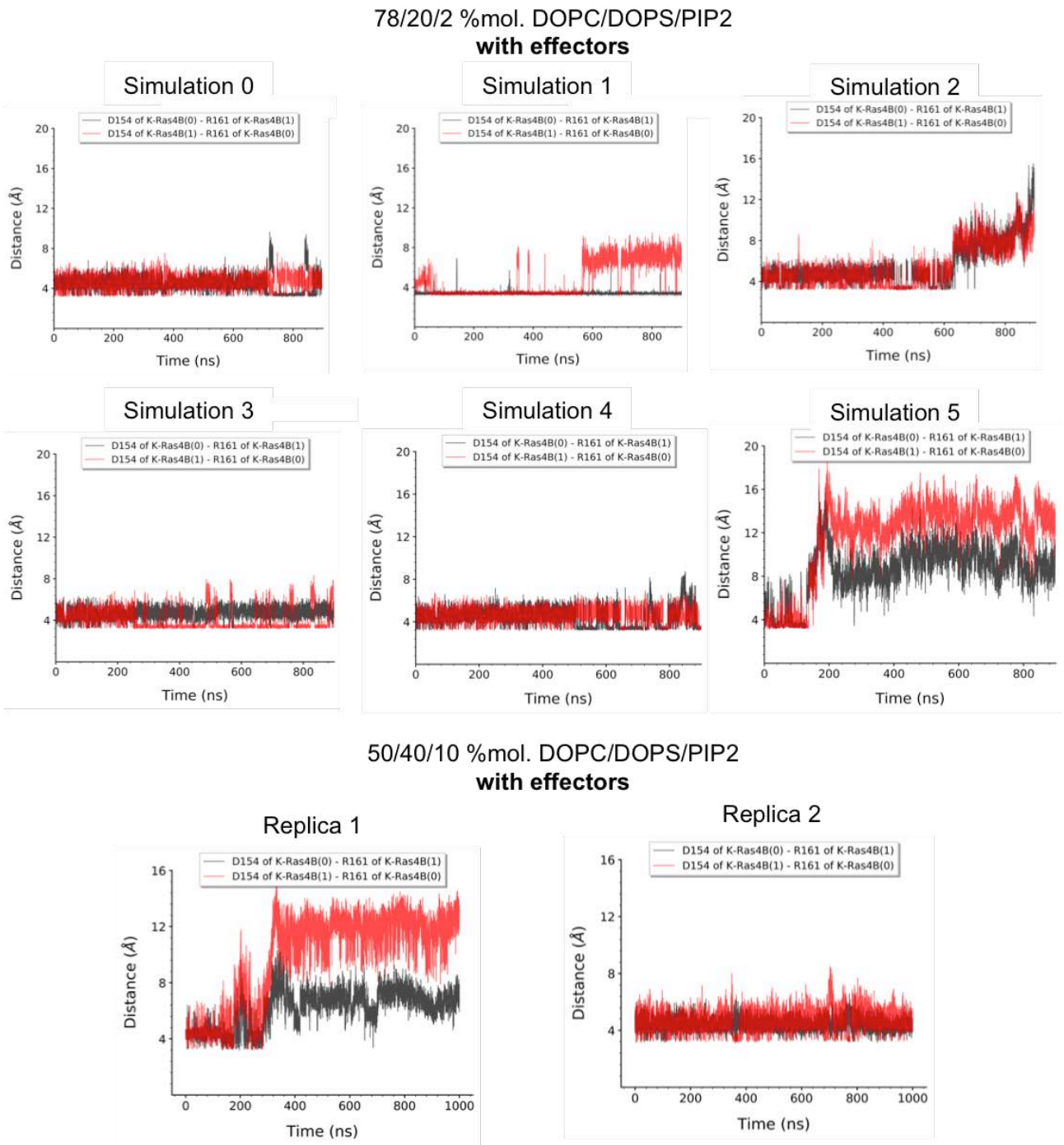

Figure 5. Distance of salt bridges between D154 and R161 for the K-Ras4B dimer on a 78:20:2 (upper panel) or a 50:40:10 membrane (lower panel) with the Raf[RBD/CRD] effectors for all independent runs.

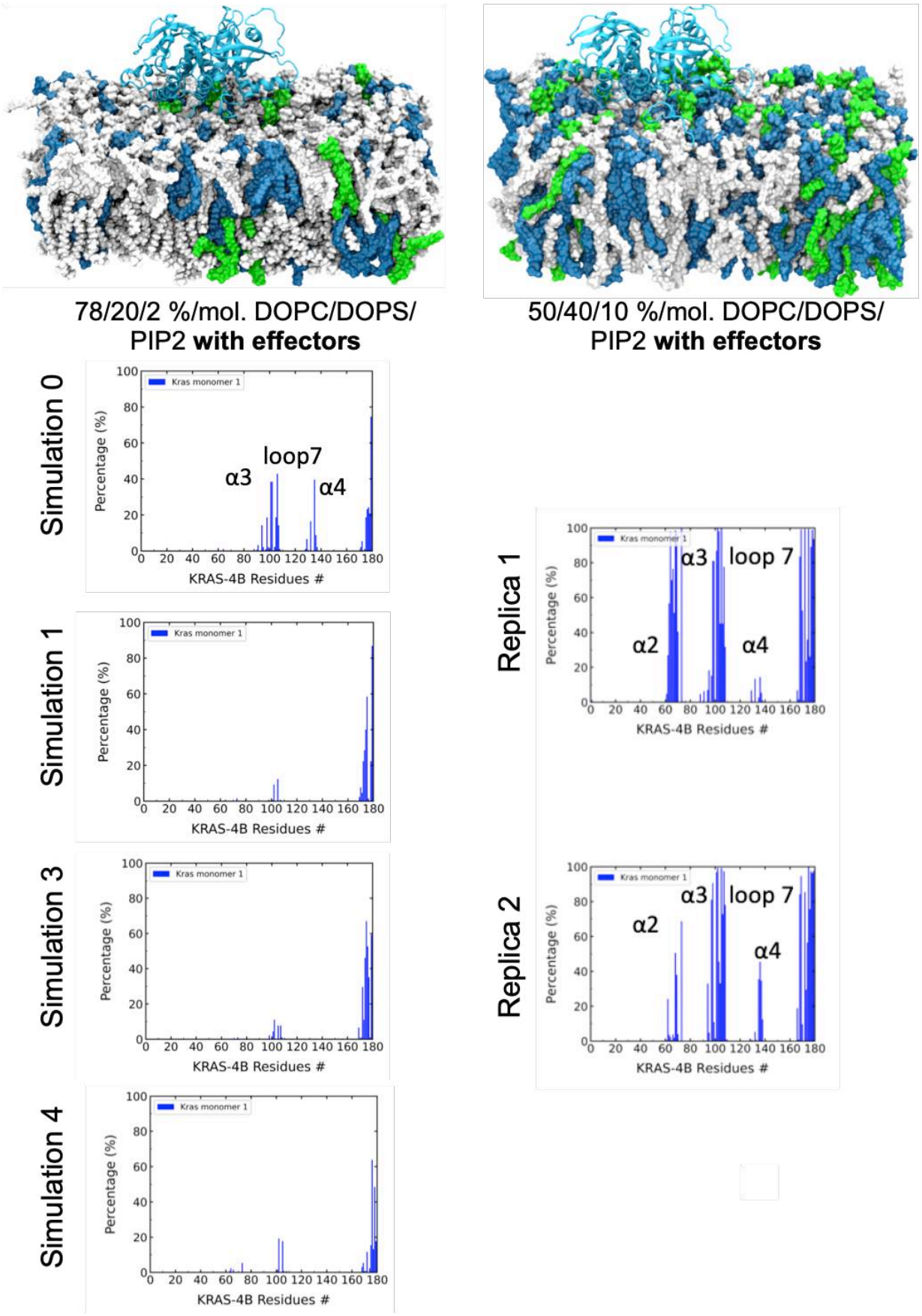

Figure 6. Orientations of K-Ras4B dimer on the membrane with Raf[RBD/CRD] effectors (upper panel). Percentage of K-Ras4B-membrane interactions of the K-Ras4B dimer based on the 5VQ2 structure with Raf[RBD/CRD] effectors in the 78:20:2 and 50:40:10 membrane for the KR1 monomer. The KR0 monomer

results can be found in the Supporting Indormation(Figures S18-S19). Effectors have been omitted for clarity.

The conformational changes of the K-Ras4B dimer in the presence of Raf[RBD/CRD] were further explored by calculating MSMs. The MSMs constructed for the 78:20:2 membrane with effectors yielded four macrostates with an average RMSD = 13.7 ± 0.6 Å. In all macrostates resulting from the MSMs at least one of the salt bridges is retained, which is in agreement with the salt bridges analysis discussed before. Moreover, two out of four macrostates showed an elevated CRD domain, corresponding to longer salt bridges (4.3 ± 0.2 Å), whereas in the most probable macrostates (State 3 with probability 44% and state 4 with probability 43%), the CRD is attached to the membrane and the salt bridges are shorter (3.9 ± 0.5 Å), although these two values are within the standard deviation of the calculation. The resulting macrostates are presented in Figure 7.

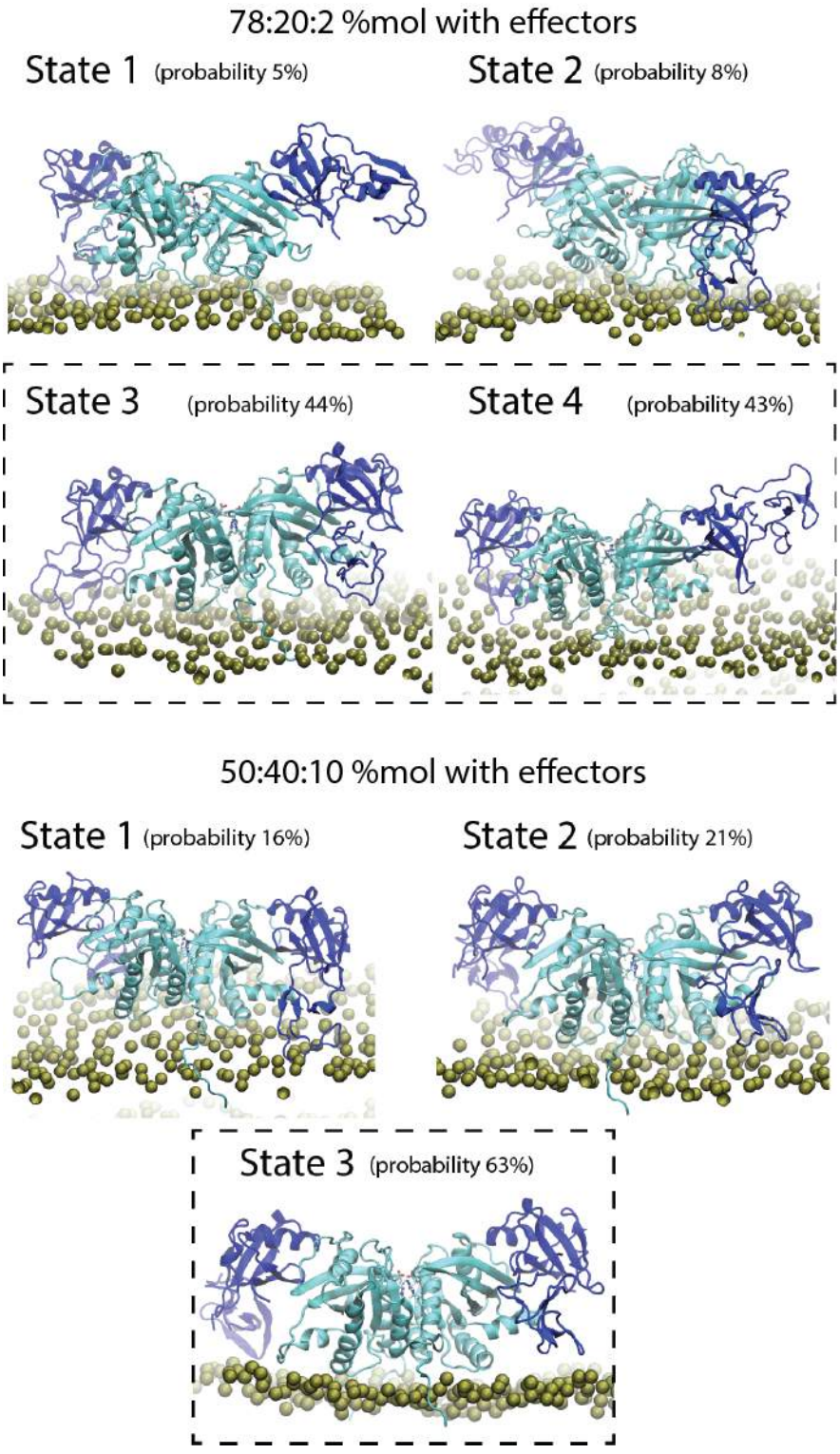

Figure 7. Metastable states of K-Ras4B/Raf[RBD/CRD] calculated by Markov State Modeling. K-Ras is depicted in cyan and Raf[RBD/CRD] is depicted in blue. For the 78:20:2 membrane with K-Ras4B effectors, the most probable conformations are State 3 (44%) and State 4 (43%), where both CRDs are attached to the membrane and the salt bridges between D154 and R161 are preserved. For the 50:40:10 membrane with K-Ras4B effectors, the most probable conformation is State 3 (63%) with stable salt bridges at the dimer interface.

In the case of 50:40:10 membrane with K-Ras4B effectors, the MSMs yielded three similar macrostates, where both CRDs are attached to the membrane, and the α2, α3 and α4 helices are tilted towards the membrane plane. In macrostate 1, only one of the salt bridges is present, while in macrostate 2 and the most probable macrostate 3 (with probability 63%), both salt bridges are present, which is in agreement with the results discussed above, for systems where the CRD is attached to the membrane.

Again, a cross-validation of the most characteristic K-Ras4B conformations took place by constructing contour plots, showing the population of states according to the K-Ras4B orientation with respect to the membrane. The results are in very good agreement with the most probable K-Ras4B conformation resulting from the MSM analysis, for both membrane models with K-Ras4B with effectors, as illustrated in Figure 8. The white rectangles represent the relevant K-Ras4B/membrane distance and K-Ras4B α5 helix/membrane plane angle for macrostate 3 and are located in the highest probability areas of the contour plot.

Furthermore, in order to monitor the Raf[CRD] orientation with respect to the α5 helix of K-Ras4B, we computed the angle between the vectors between β-sheet residues of Raf[CRD], G162 and C165, and the K-Ras4B α5 helix residues V152 and K165 (Figure S7). The results are presented in Table 1. The first 500 ns of the simulation were discarded before averaging due to high fluctuations in the observed angle. The results show that the Raf[CRD] is oriented in a range of angles from 50 to 160 degrees with respect to the α5 helix of K-Ras4B, while the small standard deviations indicate that the relative orientation is stable throughout the simulation time.

A cluster analysis in each replica trajectory (Figure S13) was performed, which shows that in both systems containing effectors, residues 166-172 of the α5 helix of each monomer are unfolded, irrespective to the membrane composition, whereas in the 78:20:2 membrane system without effectors, residues 166-172 of the α5 helix of one of the monomers is folded. When the K-Ras4B/Raf[RBD/CRD] complex is embedded in membranes with high PIP2 concentration (10% mol.), these residues are unfolded α5 helices and are leaning more towards the membrane in comparison to the systems with low PIP2 concentration (2% mol.) as illustrated in Figure S13.

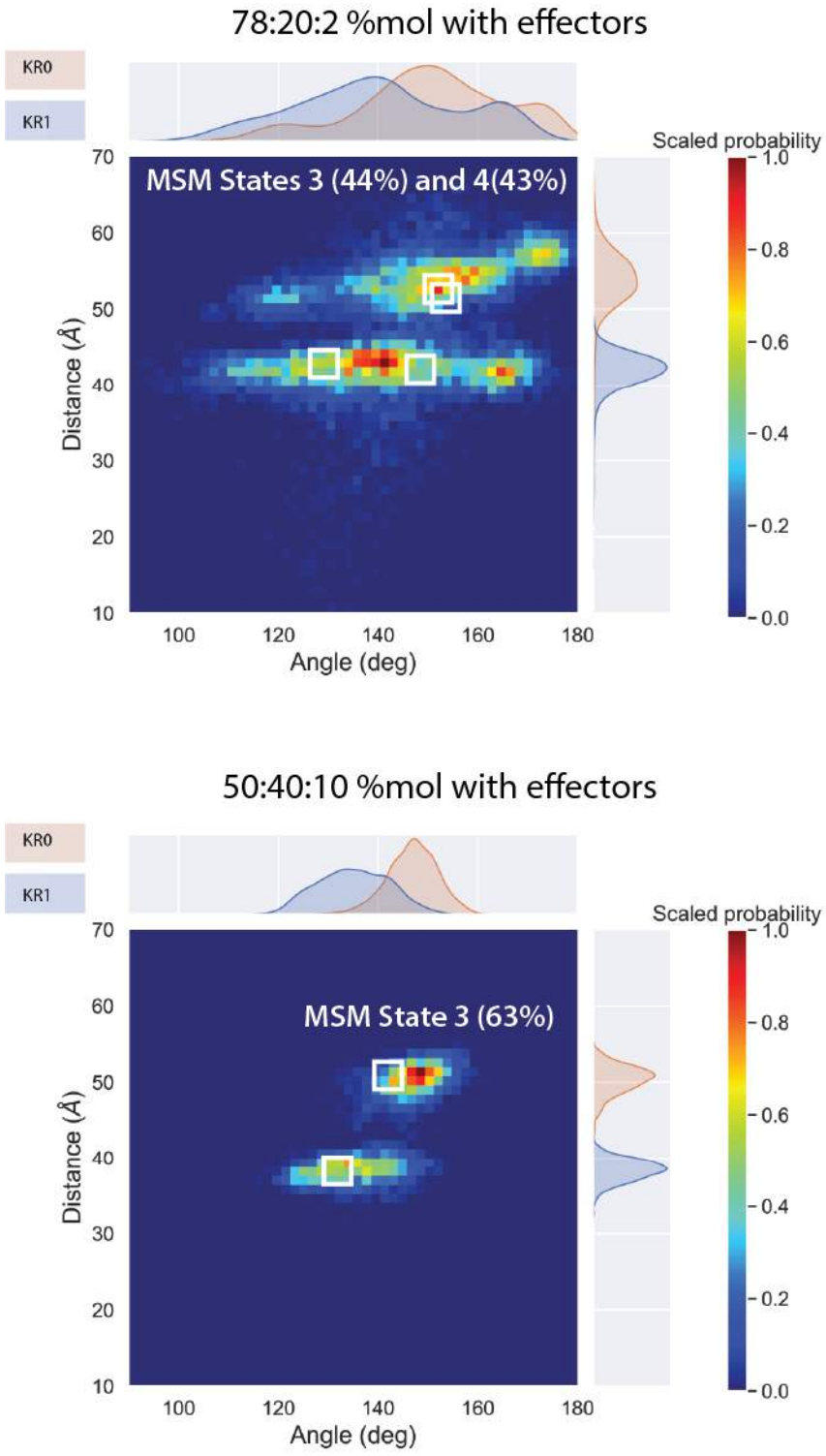

Figure 8. Contour plots showing the population of K-Ras4B states with respect to their membrane orientation for 78:20:2 (top) and 50:40:10 (bottom) membranes with Raf effectors. The computed distance corresponds to the distance between the geometric center of each K-Ras4B monomer and the bilayer geometric center, whereas the computed angle corresponds to the angle of each K-Ras4B α5 helix with respect to the membrane plane. The white rectangles correspond to the relevant distances and angles of the most probable metastable states calculated from MSMs (see the Supporting Information). Distance and angle histograms of the two K-Ras4B monomers are illustrated in pink (KR0) and light blue (KR1).

3.3 Restraining the CRD on the Membrane Does Not Confer Additional Stability to the Membrane-Bound K-Ras4B Dimer with Raf[CRD/RBD] Effectors

In the previous section it was observed that the strength of the CRD-membrane interactions seems to influence K-Ras4B dimer conformational stability. The CRD domain of Raf contains three positively charged residues, R143, K144 and K148, which form ionic interactions with the negatively charged DOPS and PIP2 lipids.[42] As shown in Ref.[57] , K148 of CRD is the most important residue responsible for the CRD-membrane binding and anchoring process. Hence, in order to evaluate whether the anchoring of the CRD domain is the decisive factor for K-Ras4B stability on the membrane, we restrained K148 to the membrane (see Table S1) and tested the effect of CRD anchoring on the 78:20:2 and 50:40:10 membranes on the stability of K-Ras4B conformation. In the 78:20:2 membrane simulations, we observed that although CRD is anchored on the membrane, it does not offer additional stability to the dimer system relative to the unconstrained system; salt bridges on the dimer interface break (R168 bound to D154) after ~500 ns in two out of three simulations (Figure S20). On the other hand, in the simulations with the 50:40:10 membrane, we observed that the dimer remains stable and the system retains these salt bridges (Figure S21). Therefore, we conclude that both the presence of the effectors with the CRDs anchoring on the membrane and the membrane composition should influence the conformational stability of the K-Ras4B dimer preserving the two interfacial R161-D154 salt bridge interactions.

Figures S22 and S23 show the percentage of contacts below 5 Å between the center of mass of each amino acid side chain of K-Ras4B (monomer 0) and K-Ras4B (monomer 1) with the center of mass of the head group of the lipid for all simulations. Compared to the simulations with unrestrained CRD for both membrane types (Figures 4, S18 and S19) we observe that membrane contacts are more limited in the 50:40:10 membrane, where K148 is restrained on the membrane. In these restrained simulations, calculations of the RMSF of K-Ras4B (Figures S24 and S25) showed that the flexibility of the switch II region is not affected.

3.4 Further Structural and Dynamical Analyses

Relationship between α5 helicity and stability of the dimer interface

We also investigated how the absence of secondary structure content of the α5 C-terminal helix affects the stability of the dimer interface. α5 helix has the potential to impose geometrical constraints on the orientation of the G-domain since the C-terminus of the α5 helix orients towards the membrane with a small tilt angle perpendicular to the membrane plane. In Figures S27, S29, S31, S33, S35 and S37, the secondary structure of residues 166-172 is plotted against simulation time for the 78:20:2 membrane with and without restraints for the two K-Ras4B monomers. Figures S26, S28, S30, S32, S34, and S36 show the secondary structure content (helix, turn, 3/10 helix) of residues 166 to 172 for the 78:20:2 membrane with and without restraints for the two K-Ras4B monomers (left: monomer 0, right: monomer 1). These plots suggest that when the secondary structure content of α5 at residues 166-172 is over 50% the R161-D154 salt bridge breaks. A relationship between the length of α5 and the orientation of the G-domain was also observed in a previous study.[27] The relationship between HVR-CRD interactions and the stability of the dimer interface was also investigated, but no correlation was found for CRD-HVR contacts and the dimer interface or the CRD leaving the membrane for the 78:20:2 or 50:40:10 membrane dimer systems with varying HVR initial positions in the membrane.

Diffusion of K-Ras4B, DOPC, DOPS and PIP2 Molecules

To characterize the effect of the membrane constitution and Raf effectors on the diffusion of K-Ras4B dimer, we computed the diffusion coefficients of K-Ras4B and the phospholipids (Figures S38-S42). K-Ras4B monomer diffusion has been experimentally measured in a 20%PS:80%PC membrane to be 3.5 $\mu m^2/s$ via single-particle trafficking techniques or 4.5 $\mu m^2/s$ if measured by fluorescence correlation spectroscopy.[56] Ngo et al.[30] have calculated the monomer K-Ras4B diffusion coefficient in presence of the Raf effector to be 3.00 ± 0.22 $\mu m^2/s$ in a membrane of 30:70 PS:PC and 2.64 ± 0.22 $\mu m^2/s$ for a membrane of 8:92 PIP2:PC. In our simulations, the K-Ras4B diffuses in a dimer form with an average Dlat = 0.39 ± 0.26 $\mu m^2/s$ without Raf effectors in the 78:20:2 membrane and 0.50 ± 0.27 $\mu m^2/s$ in the 50:40:10 membrane, showing that the K-Ras4B diffusion is independent of the lipid composition (Table 2). This finding is verified by studies performed with fluorescence measurements showing that the diffusion coefficients of eGFP−RAS on membranes with 3.3% mol. of PIP2 are only ~0.2−0.6 $\mu m^2/s$ lower than the diffusion coefficients of eGFP−RAS on membranes with 10% mol. PS, indicating that there is no significant difference in the K-Ras4B

diffusion upon change of the lipid composition.[56] Values of Dlat for all components of the systems for the different replicas are shown in Table S2.

For the K-Ras4B dimer system in the presence of Raf effectors, Dlat = 0.50 ± 0.69 $\mu m^2/s$ in a 78:20:2 membrane and Dlat = 0.12 ± 0.15 $\mu m^2/s$ in the 50:40:10 membrane. In the presence of Raf effectors and the 50:40:10 membrane, K-Ras4B is slowed down 3-fold (Dlat = 0.12 ± 0.15 $\mu m^2/s$) compared to the system without Raf effectors (0.50 ± 0.27 $\mu m^2/s$), which can be rationalized by the fact that the presence of the effectors create a bulkier system, which is more difficult to diffuse, albeit this trend is not observed in the 78:20:2 membrane. Figure S43 shows that the diffusion coefficients of K-RAS4B and PIP2 are strongly correlated, while they are not for DOPC or DOPS, a finding that is also observed in Ref.[30].

Differences in the lipid diffusion between the different systems are also observed. DOPC, DOPS and PIP2 molecules are more confined on the 50:40:10 membrane with a 2-fold slowdown in terms of lipid diffusion. Thus, lipid diffusion appears to be affected by the change in lipid concentrations.

Table 1. Number of P atoms of DOPC, DOPS, and PIP2 at 10 Å distance of the T183 Cα atom of the HVR as calculated by RDFs.

	P atom of DOPC	P atom of DOPS	P atom of PIP2
78:20:2 no effectors	2.1 ± 0.5	0.8 ± 0.5	0.6 ± 0.4
50:40:10 no effectors	1.3 ± 0.3	1.7 ± 0.6	0.6 ± 0.5
78:20:2 with effectors	2.0 ± 0.6	1.0 ± 0.6	0.4 ± 0.4
50:40:10 with effectors	1.0 ± 0.2	1.6 ± 0.5	0.4 ± 0.1

Table 2. Number of P atoms of DOPC, DOPS, and PIP2 at 10 Å distance of the NZ atom of K148 of Raf[CRD] as calculated by RDFs.

	P atom of DOPC	P atom of DOPS	P atom of PIP2
78:20:2 with effectors	2.0 ± 1.1	2.4 ± 0.9	0
50:40:10 with effectors	0.8 ± 0.8	1.5 ± 0.2	0.7 ± 0

Table 3. Average angle between the vectors consisting of the β-sheet residues of the CRD domain, G162 and C165 and the K-Ras4B α5 helix, V152 and K165.

78:20:2 with effectors	**Angle (Degrees)**	
	Dimer 0	**Dimer 1**
simulation 0	$\mathbf{109.8 \pm 5.8}$	$\mathbf{58.6 \pm 16.7}$
simulation 1	$\mathbf{117.2 \pm 3.5}$	$\mathbf{56.3 \pm 6.6}$
simulation 2	$\mathbf{99.9 \pm 41.0}$	$\mathbf{55.2 \pm 6.7}$
simulation 3	$\mathbf{89.1 \pm 6.4}$	$\mathbf{87.4 \pm 7.2}$
simulation 4	$\mathbf{156.6 \pm 10.8}$	$\mathbf{115.6 \pm 13.3}$

simulation 5	160.2 ± 7.8	136.4 ± 8.4
50:40:10 with effectors	**Angle (Degrees)**	
	Dimer 0	**Dimer 1**
Replica 1	154.9 ± 9.5	87.9 ± 9.6
Replica 2	143.4 ± 7.7	135.3 ± 8.7

Table 4. Diffusion coefficients for K-Ras4B, DOPC, DOPS and PIP2 molecules averaged over replica simulations.

Simulation	**Diffusion coefficient of K-Ras4B ($\mu m^2/s$)**	**Diffusion coefficient of DOPC ($\mu m^2/s$)**	**Diffusion coefficient of DOPS ($\mu m^2/s$)**	**Diffusion coefficient of PIP2 ($\mu m^2/s$)**
78:20:2 with effectors	0.50 ± 0.69	6.70 ± 1.08	6.69 ± 1.53	5.82 ± 1.80
78:20:2 no Effectors	0.39 ± 0.26	5.58 ± 0.32	4.94 ± 0.98	4.50 ± 1.12
50:40:10 with effectors	0.12 ± 0.15	2.91 ± 0.64	2.59 ± 0.69	2.28 ± 0.90
50:40:10 no effectors	0.50 ± 0.27	4.64 ± 0.58	2.90 ± 0.38	2.37 ± 0.71

4. Conclusions

A longstanding question in the biology of KRAS has been to determine its membrane-anchored structure, which is critical for activation of Raf kinases and thus downstream signaling. Recent evidence points to dimer conformations as the most stable membrane-anchored structure, but the exact structure of the K-Ras4B dimer has not been experimentally resolved in the presence of its effector proteins. In this study, we use microsecond all-atom MD simulations to investigate how K-Ras4B spatiotemporal properties are affected by two different membranes differing in their percentage of anionic lipids in the absence and presence of Raf[CRD-RBD] effectors.

First, we construct the K-Ras4B dimer based on the 5VQ2 crystal structure and verify its stability over other orientations through independent simulations. Then, we construct two model membranes with a lipid composition of 78% mol. DOPC, 20% mol. DOPS, and 2% mol. PIP2 (78:20:2 membrane) and one with a higher concentration of the negatively charged DOPS and PIP2 lipids, namely 50% mol. DOPC, 40% mol. DOPS, and 10% mol. PIP2 (50:40:10 membrane) in order to monitor the spatiotemporal stability of the dimer in the presence and absence of Raf[CRD-RBD] effectors. Our simulations reveal that when the membrane is enriched with negatively charged phospholipids, the K-Ras4B dimer remains stable on the

membrane independent of the presence of the effectors. The role of anionic lipids in the cellular membrane and PIP2 in particular has also been highlighted by numerous previous studies.[30,32,34,35, 40] Specifically, clustering of PIP2 molecules has been observed in the vicinity of K-Ras4A where several PIP2 molecules were found to interact with positively charged residues of K-Ras.[40] The preference of K-Ras4B binding the PIP2 lipids has been also shown by simulations of the K-Ras4B monomer in different composition model membranes in a recent study[30] and is also supported by experimental results.[35,58] Contradictory experimental results also exist,[29] which showed that K-Ras4B may prefer co-localizing with PS than with PIP2 in lipid membranes having less than 1% of PIP2, versus 10-20% of PS, however this low average cellular concentration of PIP2 may not be characteristic of the actual membrane environment, since PIP2, similarly to other phosphoinositides, engages in a non-uniform distribution in the plasma membrane.[31]

The conformational flexibility of the K-Ras4B dimer in the 78:20:2 membrane in the absence of effectors triggers an overall instability of the interactions along the dimer interface, including loss of the salt bridge between D154 and R161 at the dimer interface. This disruption of the α4-α5 dimer interface is observed in all replica simulations and confirmed by MSM analysis. These observations are in close agreement with reported studies suggesting that K-Ras4B gains dimerization capability only in the presence of additional factors, i.e. downstream effectors such as Raf.[56] As an additional factor contributing to K-Ras4B stable dimers we report here that an increased concentration of anionic lipids (50:40:10 membrane) can confer stability to that α4/α5 K-Ras4B dimer interface (facilitated by the D14-R1616 salt bridge) even in the absence of effector binding (Figure 2). Indeed, while we find that K-Ras4B diffusion is not influenced by the PIP2 concentration, K-Ras4B diffusion is correlated to the diffusion of PIP2 but not to DOPS or DOPC, which could indicate a stabilizing PIP2 effect. Further studies on K-RAS protein-protein interactions suggest that although the catalytic domain is directly involved in the dimer formation, the interactions are so weak that dimers are unlikely to be observed under standard experimental conditions, but can be enriched upon membrane binding.[59] This conclusion could also imply that the effector recruitment together with the stable binding of the complex on the membrane is of vital importance for K-RAS dimerization.

Regarding the relative orientation of the K-Ras4B dimer with respect to the plane of the membrane in the presence and absence of effectors and the tow model membranes, we made the following observations. For the 78:20:2 membrane in the absence of effectors, the disrupted dimer adopts a tilted conformation towards the membrane with angles of the α5 helix with respect to the bilayer plane ranging from 130 to 150 degrees (Figure 4). In the presence of effectors in the 78:20:2 membrane, the α5 helices angle with respect to the bilayer plane adopt higher values (140 to 160 degrees, shown in Figure 8), which can be attributed to the fact that the effectors detach from the membrane and force one of the α5 helices to adopt conformations in a wider angle. In the case of the 50:40:10 membrane, the system without effectors swings between a significantly tilted conformation that can reach up to 115 degrees angle between the α5 helix

and the membrane plane and a less tilted conformation of 140 degrees (Figure 4). In the presence of effectors the system is further stabilized and adopts conformations with angle values of 140-150 degrees, indicating that the effectors restrict the dimmer tilt towards the membrane. Moreover, the additional negative charge of the 50:40:10 membrane results in a more confined K-Ras4B geometric center/membrane geometric center distance distribution in comparison with the 78:20:2 model, as shown in the distance histograms of Figure 4 and Figure 8.

We also investigated how the secondary structure of the C-terminus of the α5 helix affects the stability of the dimer interface and observed that when the secondary structure content of α5 helix residues 166-172 is over 50%, the R161-D154 salt bridge breaks. Indeed, the α5 helix has the potential to impose geometrical constraints on the orientation of the G-domain since the C-terminus of the α5 helix extends to the HRV in direct contact with the membrane. We conclude that the α5 helix needs to be unfolded beyond residue 166 in order for the α4/α5 dimer interface to be restrained, although several crystal structures show α5 helical extension to HRV residue K172 (PDB ID: 6GOD[60]) or D173 (PDB ID: 4DSO[44]). Other studies have also observed that α5 helix may lose 50% of its helicity at residue K167 during the course of the simulations.[27]

We observe that the stabilizing factor of the K-Ras4B dimer in the presence of the Raf effectors is the ability of the Raf[CRD] domains to remain anchored on the membrane. This is in agreement with a recent study combining biophysical and computational methods, which showed that the membrane-anchored K-RAS populates a membrane distal conformation, which allows the recruitment of Raf, pinpointing the importance of the membrane anchor. This study suggests that such observations are compatible with a directional fly-casting mechanism for K-Ras4B, in which the membrane-distal state of the G-domain can effectively recruit Raf kinase from the cytoplasm for activation at the membrane.[61] Despite its importance, HVR anchoring alone does not suffice for K-Ras4B dimerization, as suggested by fluorescence correlation spectroscopy experiments on supported membranes.[56] In a similar fashion, according to our study, K-Ras4B interface salt bridges are stable in the 50:40:10 membrane only if Raf[CRD] domains are stable on the model membrane, indicating that the additional negatively charged lipids do not confer additional stability to the α4-α5 K-Ras4B interface in the presence of Raf[RBD/CRD] effectors. The stabilities of the K-Ras4B dimer with Raf[RBD/CRD] effectors in the 78:20:2 and 50:40:10 membrane does not differ significantly, including the stability of the D154 and R161 dimer salt bridges, indicating that in the presence of Raf effectors the desired dimer stability is reached without being influenced by anionic lipid concentration. A recent study using a combination of size exclusion chromatography (SEC) and small angle X-ray scattering (SAXS) experiments indicates that the presence of Raf[RBD] is sufficient to promote Ras G-domain dimerization, even in the absence of membrane or the HVR, highlighting the importance of Raf[RBD]binding for the stability of the K-Ras dimer.[25] In the same study, single molecule tracking experiments and fluorescence correlation spectroscopy have shown that Raf[RBD] is of vital importance for robust

dimerization of Ras on supported membranes. Furthermore, allosteric network analysis of MD simulations indicated that dimerization dramatically increases allosteric connections, connecting the two Raf[RBD] molecules at opposite ends of the dimer formed by the α4-α5 interface of the K-Ras monomers.[25] Strong allosteric connection between Ras G-domain and Raf effectors has also been observed for the Q61L Ras mutant.[24]

We finally conclude that both anchoring of Raf[CRD] on the membrane and the membrane composition are decisive factors determining the K-Ras4B dimer stability. The results reported herein have provided with an insight on the effects of both the membrane environment and the Raf binding with respect to the stabilization of the K-Ras dimers formed through an α4-α5 interface. Further studies combining the atomistic detail of molecular simulations with experimental validation using biophysical and biochemical assays are needed in order to shed light upon this complicated mechanism of Raf/Ras activation.

Acknowledgements

This work was supported by computational time granted from the Greek Research & Technology Network (GRNET) in the National HPC facility—ARIS—under Project IDs pr008031_thin/KRAS and pr009022_gpu/KRAS-MEM. This research work was supported by the Hellenic Foundation for Research and Innovation (H.F.R.I.) under the "First Call for H.F.R.I. Research Projects to support Faculty members and Researchers and the procurement of high-cost research equipment grant" (Project Number: 1780) awarded to ZC. The authors thank Dr. Michalis Papadourakis for help with the analysis.

Corresponding Author

Zoe Cournia, E-mail: zcournia@bioacademy.gr

José S Duca, E-mail: jose.duca@novartis.com

Author contributions

The manuscript was written through contributions of all authors. All authors have given approval to the final version of the manuscript.

Competing interests

The authors declare no competing financial interest.

Supporting Information

Methods; lists of simulations, diffusion coefficients, and MSM parameters (Tables S1−S3); Ras dimerization conformation, structures, Chapman−Kolmogorov tests, timescales vs lag time and energy surfaces, RMSD time series and dimer simulations, percentage or orientations, membrane interactions, and membrane contacts vs number of residues, RMSF of the dimer and amino acids, distance vs time for salt bridges, secondary structure vs simulation time, frequency of the existence of a secondary structure element, mean square displacement plot and log(MSD(t))/log(t) plots, and correlation of lateral diffusion (Figures S1−S43) (PDF).

PDB files of cluster representatives and MSM states (ZIP).

References

1. Vetter, I. R.; Wittinghofer, A., The Guanine Nucleotide-Binding Switch in Three Dimensions. *Science* **2001,** *294* (5545), 1299-1304.
2. Bos, J. L.; Rehmann, H.; Wittinghofer, A., GEFs and GAPs: Critical Elements in the Control of Small G Proteins. *Cell* **2007,** *129* (5), 865-77.
3. Prior, I. A.; Lewis, P. D.; Mattos, C., A Comprehensive Survey of Ras Mutations in Cancer. *Cancer Res.* **2012,** *72* (10), 2457-67.
4. Cox, A. D.; Fesik, S. W.; Kimmelman, A. C.; Luo, J.; Der, C. J., Drugging the Undruggable RAS: Mission Possible? *Nat Rev Drug Discov.* **2014,** *13* (11), 828-51.
5. Wittinghofer, A.; Vetter, I. R., Structure-Function Relationships of the G Domain, a Canonical Switch Motif. *Annu. Rev. Biochem.* **2011,** *80*, 943-971.
6. Laude, A. J.; Prior, I. A., Palmitoylation and Localisation of RAS Isoforms are Modulated by the Hypervariable Linker Domain. *Journal of Cell Science* **2008,** *121* (Pt 4), 421-427.
7. Welman, A.; Burger, M. M.; Hagmann, J., Structure and Function of the C-terminal Hypervariable Region of K-Ras4B in Plasma Membrane Targetting and Transformation. *Oncogene* **2000,** *19* (40), 4582-4591.
8. Leevers, S. J.; Paterson, H. F.; Marshall, C. J., Requirement for Ras in Raf Activation is Overcome by Targeting Raf to the Plasma Membrane. *Nature* **1994,** *369* (6479), 411-414.
9. Kholodenko, B. N.; Hancock, J. F.; Kolch, W., Signalling Ballet in Space and Time. *Nat. Rev. Mol. Cell Biol.* **2010,** *11* (6), 414-426.
10. Stokoe, D.; Macdonald, S. G.; Cadwallader, K.; Symons, M.; Hancock, J. F., Activation of Raf as a Result of Recruitment to the Plasma Membrane. *Science* **1994,** *264* (5164), 1463-1467.
11. Nassar, N.; Horn, G.; Herrmann, C. A.; Scherer, A.; McCormick, F.; Wittinghofer, A., The 2.2 Å Crystal Structure of the Ras-Binding Domain of the Serine/Threonine Kinase c-Raf1 in Complex with RaplA and a GTP Analogue. *Nature* **1995,** *375* (6532), 554-560.

12. Hekman, M.; Hamm, H.; Villar, A. V.; Bader, B.; Kuhlmann, J.; Nickel, J.; Rapp, U. R., Associations of B- and C-Raf with Cholesterol, Phosphatidylserine, and Lipid Second Messengers: PREFERENTIAL BINDING OF Raf TO ARTIFICIAL LIPID RAFTS. *J. Biol. Chem.* **2002,** *277* (27), 24090-102.
13. Dougherty, M. K.; Müller, J.; Ritt, D. A.; Zhou, M.; Zhou, X. Z.; Copeland, T. D.; Conrads, T. P.; Veenstra, T. D.; Lu, K. P.; Morrison, D. K., Regulation of Raf-1 by Direct Feedback Phosphorylation. *Mol. Cell* **2005,** *17* (2), 215-224.
14. Nan, X.; Tamgüney, T. M.; Collisson, E. A.; Lin, L.-J.; Pitt, C.; Galeas, J.; Lewis, S.; Gray, J. W.; McCormick, F.; Chu, S., Ras-GTP Dimers Activate the Mitogen-Activated Protein Kinase (MAPK) Pathway. *Proc. Natl. Acad. Sci. U. S. A.* **2015,** *112* (26), 7996-8001.
15. Muratcioglu, S.; Chavan, T. S.; Freed, B. C.; Jang, H.; Khavrutskii, L.; Freed, R. N.; Dyba, M. A.; Stefanisko, K.; Tarasov, S. G.; Gursoy, A.; Keskin, O.; Tarasova, N. I.; Gaponenko, V.; Nussinov, R., GTP-Dependent K-Ras Dimerization. *Structure* **2015,** *23* (7), 1325-35.
16. Ambrogio, C.; Köhler, J.; Zhou, Z.-W.; Wang, H.; Paranal, R.; Li, J.; Capelletti, M.; Caffarra, C.; Li, S.; Lv, Q.; Gondi, S.; Hunter, J. C.; Lu, J.; Chiarle, R.; Santamaria, D.; Westover, K. D.; Jänne, P. A., KRAS Dimerization Impacts MEK Inhibitor Sensitivity and Oncogenic Activity of Mutant KRAS. *Cell* **2018,** *172* (4), 857-868 e15.
17. Lee, K.-Y.; Fang, Z.; Enomoto, M.; Gasmi-Seabrook, G.; Zheng, L.; Koide, S.; Ikura, M.; Marshall, C. B., Two Distinct Structures of Membrane-Associated Homodimers of GTP- and GDP-Bound KRAS4B Revealed by Paramagnetic Relaxation Enhancement. *Angew Chem Int Ed* **2020,** *59* (27), 11037-11045.
18. Barklis, E.; Stephen, A. G.; Staubus, A. O.; Barklis, R. L.; Alfadhli, A., Organization of Farnesylated, Carboxymethylated KRAS4B on Membranes. *Journal of molecular biology* **2019,** *431* (19), 3706-3717.
19. Güldenhaupt, J.; Rudack, T.; Bachler, P.; Mann, D.; Triola, G.; Waldmann, H.; Kötting, C.; Gerwert, K., N-Ras Forms Dimers at POPC Membranes. *Biophys. J.* **2012,** *103* (7), 1585-1593.
20. Spencer-Smith, R.; Koide, A.; Zhou, Y.; Eguchi, R. R.; She, F.; Gajwani, P.; Santana, D.; Gupta, A.; Jacobs, M.; Herrero-Garcia, E.; Cobbert, J.; Lavoie, H.; Smith, M.; Rajakulendran, T.; Dowdell, E.; Okur, M. N.; Dementieva, I.; Sicheri, F.; Therrien, M.; Hancock, J. F.; Ikura, M.; Koide, S.; O'Bryan, J. P., Inhibition of RAS Function Through Targeting an Allosteric Regulatory Site. *Nature Chemical Biology* **2017,** *13* (1), 62-68.
21. Cookis, T.; Mattos, C., Crystal Structure Reveals the Full Ras:Raf Interface and Advances Mechanistic Understanding of Raf Activation. *bioRxiv* **2020**, 2020.07.28.225938.
22. Jang, H.; Zhang, M.; Nussinov, R., The Quaternary Assembly of KRas4B with Raf-1 at the Membrane. *Comput. Struct. Biotechnol. J.* **2020,** *18*, 737-748.
23. Xu, S. Y.; Long, B. N.; Boris, G. H.; Chen, A. Q.; Ni, S. S.; Kennedy, M. A., Structural insight into the rearrangement of the switch I region in GTP-bound G12A K-Ras. *Acta Crystallogr. D* **2017,** *73* (12), 970-984.
24. Fetics, S. K.; Guterres, H.; Kearney, B. M.; Buhrman, G.; Ma, B.; Nussinov, R.; Mattos, C., Allosteric Effects of the Oncogenic RasQ61L Mutant on Raf-RBD. *Structure* **2015,** *23* (3), 505-516.
25. Packer, M. R.; Parker, J. A.; Chung, J. K.; Li, Z.; Lee, Y. K.; Cookis, T.; Guterres, H.; Alvarez, S.; Hossain, M. A.; Donnelly, D. P.; Agar, J. N.; Makowski, L.; Buck, M.; Groves, J. T.; Mattos, C., Raf promotes dimerization of the Ras G-domain with increased allosteric connections. *Proc. Natl. Acad. Sci. U. S. A.* **2021,** *118* (10), e2015648118.
26. Prakash, P.; Zhou, Y.; Liang, H.; Hancock, J. F.; Gorfe, A. A., Oncogenic K-Ras Binds to an Anionic Membrane in Two Distinct Orientations: A Molecular Dynamics Analysis. *Biophys. J.* **2016,** *110* (5), 1125-38.
27. Neale, C.; García, A. E., The Plasma Membrane as a Competitive Inhibitor and Positive Allosteric Modulator of KRas4B Signaling. *Biophys. J.* **2020,** *118* (5), 1129-1141.
28. Mazhab-Jafari, M. T.; Marshall, C. B.; Smith, M. J.; Gasmi-Seabrook, G. M. C.; Stathopulos, P. B.; Inagaki, F.; Kay, L. E.; Neel, B. G.; Ikura, M., Oncogenic and RASopathy-Associated K-RAS Mutations Relieve Membrane-Dependent Occlusion of the Effector-Binding Site. *Proc. Natl. Acad. Sci. U. S. A.* **2015,** *112* (21), 6625-6630.
29. Zhou, Y.; Prakash, P.; Liang, H.; Cho, K.-J.; Gorfe, A. A.; Hancock, J. F., Lipid-Sorting Specificity Encoded in K-Ras Membrane Anchor Regulates Signal Output. *Cell* **2017,** *168* (1-2), 239-251.e16.
30. Ngo, V. A.; Sarkar, S.; Neale, C.; Garcia, A. E., How Anionic Lipids Affect Spatiotemporal Properties of KRAS4B on Model Membranes. *J Phys Chem B* **2020,** *124* (26), 5434-5453.
31. McLaughlin, S.; Wang, J.; Gambhir, A.; Murray, D., PIP(2) and Proteins: Interactions, Organization, and Information Flow. *Annu. Rev. Biophys. Biomol. Struct.* **2002,** *31*, 151-175.
32. Alvarez-Moya, B.; Barceló, C.; Tebar, F.; Jaumot, M.; Agell, N., CaM Interaction and Ser181 Phosphorylation as new K-Ras Signaling Modulators. *Small GTPases* **2011,** *2* (2), 99-103.

33. McLean, M. A.; Stephen, A. G.; Sligar, S. G., PIP2 Influences the Conformational Dynamics of Membrane-Bound KRAS4b. *Biochemistry* **2019,** *58* (33), 3537-3545.
34. Cao, S.; Chung, S.; Kim, S.; Li, Z.; Manor, D.; Buck, M., K-Ras G-Domain Binding with Signaling Lipid Phosphatidylinositol (4,5)-Phosphate (PIP2): Membrane Association, Protein Orientation, and Function. *J. Biol. Chem.* **2019,** *294* (17), 7068-7084.
35. Gregory, M. C.; McLean, M. A.; Sligar, S. G., Interaction of KRas4b with Anionic Membranes: A Special Role for PIP2. *Biochem. Biophys. Res. Commun.* **2017,** *487* (2), 351-355.
36. Neale, C.; García, A. E., Methionine 170 is an Environmentally Sensitive Membrane Anchor in the Disordered HVR of K-Ras4B. *J Phys Chem B* **2018,** *122* (44), 10086-10096.
37. Katan, M.; Cockcroft, S., Phosphatidylinositol(4,5)bisphosphate: Diverse Functions at the Plasma Membrane. *Essays Biochem.* **2020,** *64* (3), 513-531.
38. van den Bogaart, G.; Meyenberg, K.; Diederichsen, U.; Jahn, R., Phosphatidylinositol 4,5-Bisphosphate Increases Ca2+ Affinity of Synaptotagmin-1 by 40-Fold. *J. Biol. Chem.* **2012,** *287* (20), 16447-16453.
39. Sengupta, P.; Seo, A. Y.; Pasolli, H. A.; Song, Y. E.; Johnson, M. C.; Lippincott-Schwartz, J., A Lipid-Based Partitioning Mechanism for Selective Incorporation of Proteins into Membranes of HIV Particles. *Nature Cell Biology* **2019,** *21* (4), 452-461.
40. Li, Z.-L.; Buck, M., Computational Modeling Reveals that Signaling Lipids Modulate the Orientation of K-Ras4A at the Membrane Reflecting Protein Topology. *Structure* **2017,** *25* (4), 679-689.e2.
41. Fang, Z.; Lee, K.-Y.; Huo, K.-G.; Gasmi-Seabrook, G.; Zheng, L.; Moghal, N.; Tsao, M.-S.; Ikura, M.; Marshall, C. B., Multivalent Assembly of KRAS with the RAS-Binding and Cysteine-Rich Domains of CRAF on the Membrane. *Proc. Natl. Acad. Sci. U. S. A.* **2020,** *117* (22), 12101-12108.
42. Li, Z.-L.; Prakash, P.; Buck, M., A "tug of war" maintains a dynamic protein–membrane complex: molecular dynamics simulations of C-Raf RBD-CRD bound to K-Ras4B at an anionic membrane. *ACS Cent. Sci.* **2018,** *4* (2), 298-305.
43. Fang, Z.; Marshall, C. B.; Nishikawa, T.; Gossert, A. D.; Jansen, J. M.; Jahnke, W.; Ikura, M., Inhibition of K-RAS4B by a Unique Mechanism of Action: Stabilizing Membrane-Dependent Occlusion of the Effector-Binding Site. *Cell Chem Biol* **2018,** *25* (11), 1327-1336.e4.
44. Maurer, T.; Garrenton, L. S.; Oh, A.; Pitts, K.; Anderson, D. J.; Skelton, N. J.; Fauber, B. P.; Pan, B.; Malek, S.; Stokoe, D.; Ludlam, M. J.; Bowman, K. K.; Wu, J.; Giannetti, A. M.; Starovasnik, M. A.; Mellman, I.; Jackson, P. K.; Rudolph, J.; Wang, W.; Fang, G., Small-Molecule Ligands
Bind to a Distinct Pocket in Ras and Inhibit SOS-Mediated Nucleotide Exchange Activity. *Proc. Natl. Acad. Sci. U. S. A.* **2012,** *109* (14), 5299-5304.
45. Mott, H. R.; Carpenter, J. W.; Zhong, S.; Ghosh, S.; Bell, R. M.; Campbell, S. L., The solution structure of the Raf-1 cysteine-rich domain: a novel ras and phospholipid binding site. *Proc. Natl. Acad. Sci. U. S. A.* **1996,** *93* (16), 8312-7.
46. Tran, T. H.; Chan, A. H.; Young, L. C.; Bindu, L.; Neale, C.; Messing, S.; Dharmaiah, S.; Taylor, T.; Denson, J.-P.; Esposito, D.; Nissley, D. V.; Stephen, A. G.; McCormick, F.; Simanshu, D. K., KRAS Interaction with RAF1 RAS-Binding Domain and Cysteine-Rich Domain Provides Insights into RAS-Mediated RAF Activation. *Nat. Commun.* **2021,** *12* (1), 1176.
47. Harvey, M. J.; Giupponi, G.; Fabritiis, G. D., ACEMD: Accelerating Biomolecular Dynamics in the Microsecond Time Scale. *J. Chem. Theory Comput.* **2009,** *5* (6), 1632-1639.
48. Huang, J.; Rauscher, S.; Nawrocki, G.; Ran, T.; Feig, M.; de Groot, B. L.; Grubmüller, H.; MacKerell, A. D., Jr., CHARMM36m: an Improved Force Field for Folded and Intrinsically Disordered Proteins. *Nature methods* **2017,** *14* (1), 71-73.
49. Scherer, M. K.; Trendelkamp-Schroer, B.; Paul, F.; Pérez-Hernández, G.; Hoffmann, M.; Plattner, N.; Wehmeyer, C.; Prinz, J.-H.; Noé, F., PyEMMA 2: A Software Package for Estimation, Validation, and Analysis of Markov Models. *J. Chem. Theory Comput.* **2015,** *11* (11), 5525-5542.
50. Weber, M.; Kube, S. In *Robust Perron Cluster Analysis for Various Applications in Computational Life Science*, Computational Life Sciences, Berlin, Heidelberg, 2005//; R. Berthold, M.; Glen, R. C.; Diederichs, K.; Kohlbacher, O.; Fischer, I., Eds. Springer Berlin Heidelberg: Berlin, Heidelberg, 2005; pp 57-66.
51. Prinz, J.-H.; Wu, H.; Sarich, M.; Keller, B.; Senne, M.; Held, M.; Chodera, J. D.; Schütte, C.; Noé, F., Markov Models of Molecular Kinetics: Generation and Validation. *J. Chem. Phys.* **2011,** *134* (17), 174105.

52. Abraham, M. J.; Murtola, T.; Schulz, R.; Páll, S.; Smith, J. C.; Hess, B.; Lindahl, E., GROMACS: High Performance Molecular Simulations through Multi-Level Parallelism from Laptops to Supercomputers. *SoftwareX* **2015,** *1-2*, 19-25.
53. Kiriakidi, S.; Chatzigiannis, C.; Papaemmanouil, C.; Tzakos, A. G.; Cournia, Z.; Mavromoustakos, T., Interplay of Cholesterol, Membrane Bilayers and the AT1R: A Cholesterol Consensus Motif on AT1R is Revealed. *Comput. Struct. Biotechnol. J.* **2021,** *19*, 110-120.
54. Humphrey, W.; Dalke, A.; Schulten, K., VMD: Visual Molecular Dynamics. *J. Mol. Graph.* **1996,** *14* (1), 33-38.
55. Frishman, D. A., P., Knowledge-Based Protein Secondary Structure Assignment. *Proteins* **1995,** *23* (4), 566-579.
56. Chung, J. K.; Lee, Y. K.; Denson, J.-P.; Gillette, W. K.; Alvarez, S.; Stephen, A. G.; Groves, J. T., K-Ras4B Remains Monomeric on Membranes over a Wide Range of Surface Densities and Lipid Compositions. *Biophys. J.* **2018,** *114* (1), 137-145.
57. Li, S.; Jang, H.; Zhang, J.; Nussinov, R., Raf-1 cysteine-rich domain increases the affinity of K-Ras/Raf at the membrane, promoting MAPK signaling. *Structure* **2018,** *26* (3), 513-525. e2.
58. McLean, M. A.; Gregory, M. C.; Sligar, S. G., Nanodiscs: A Controlled Bilayer Surface for the Study of Membrane Proteins. *Annu. Rev. Biophys.* **2018,** *47* (1), 107-124.
59. Prakash, P.; Sayyed-Ahmad, A.; Cho, K.-J.; Dolino, D. M.; Chen, W.; Li, H.; Grant, B. J.; Hancock, J. F.; Gorfe, A. A., Computational and Biochemical Characterization of Two Partially Overlapping Interfaces and Multiple Weak-Affinity K-Ras Dimers. *Sci. Rep.* **2017,** *7* (1), 40109.
60. Cruz-Migoni, A.; Canning, P.; Quevedo, C. E.; Bataille, C. J. R.; Bery, N.; Miller, A.; Russell, A. J.; Phillips, S. E. V.; Carr, S. B.; Rabbitts, T. H., Structure-Based Development of New RAS-Effector Inhibitors from a Combination of Active and Inactive RAS-Binding Compounds. *Proceedings of the National Academy of Sciences* **2019,** *116* (7), 2545-2550.
61. Van, Q. N.; López, C. A.; Tonelli, M.; Taylor, T.; Niu, B.; Stanley, C. B.; Bhowmik, D.; Tran, T. H.; Frank, P. H.; Messing, S.; Alexander, P.; Scott, D.; Ye, X.; Drew, M.; Chertov, O.; Lösche, M.; Ramanathan, A.; Gross, M. L.; Hengartner, N. W.; Westler, W. M.; Markley, J. L.; Simanshu, D. K.; Nissley, D. V.; Gillette, W. K.; Esposito, D.; McCormick, F.; Gnanakaran, S.; Heinrich, F.; Stephen, A. G., Uncovering a Membrane-Distal Conformation of KRAS Available to Recruit RAF to the Plasma Membrane. *Proc. Natl. Acad. Sci. U. S. A.* **2020,** *117* (39), 24258-24268.